Yamamoto *et al.*
*Progress in Earth and Planetary Science* 2022, **9**(1):32
https://doi.org/10.1186/s40645-022-00493-4

Progress in Earth and Planetary Science

RESEARCH ARTICLE

Open Access

# Seismicity distribution in the Tonankai and Nankai seismogenic zones and its spatiotemporal relationship with interplate coupling and slow earthquakes

Yojiro Yamamoto[1*], Shuichiro Yada[1], Keisuke Ariyoshi[1], Takane Hori[1] and Narumi Takahashi[2]

## Abstract

We conducted seismic tomography to estimate the seismic velocity structure and to evaluate the spatiotemporal distribution of interplate earthquakes of the Kii Peninsula, central Honshu, Japan, where the Tonankai and Nankai megathrusts are located. Microearthquakes were quantitatively detected by using the data from a cable-type seafloor seismic observation network, completed in 2015. Our velocity model was consistent with the previous 2-D active-source surveys, which reported the areal extent of key structures: a high-velocity zone beneath Cape Shionomisaki, a subducted seamount off Cape Muroto, and the subducted Paleo-Zenith Ridge. The absence of any other subducted seamount with the same or larger spatial scale, than the identified key structures, was confirmed. Our velocity model also revealed that there was not a simple relationship between areas of large coseismic slip or strong interplate coupling and areas of high velocity in the overriding plate. Relocated hypocenters widely ranged from the upper plate to within the slab, while the most active region was attributed to the oceanic crust in the aftershock region of 2004 off-Kii earthquake. Compared with the results from the land-based observation network, the accuracy of the focal depth estimation was substantially improved. Furthermore, we identified the seismic activity in the vicinity of the plate boundary and determined 14 locations for interplate seismicity areas. They were primarily distributed in the range of seismogenic zone temperature (150–350 °C) along the plate boundary and were located outside of the strong interplate coupling zone. Several active areas of interplate earthquakes exhibited clustered activity during the periods of slow-slip events, observed and accompanied with shallow very-low-frequency earthquakes. Thus, regular interplate microearthquakes became active at the plate boundary in the conjunction with slow slip. In summary, as regular earthquakes provide a more accurate source location than slow earthquakes and can detect events of smaller magnitude, monitoring such interplate earthquakes may reveal spatiotemporal variations in the stick–slip conditions on the plate boundary.

**Keywords:** Nankai Trough subduction zone, Seismicity, Seismic velocity structure, Philippine Sea Plate, Interplate coupling, Slow earthquakes

## 1 Introduction

The plate boundary between the subducted Philippine Sea Plate and overriding Amur Plate is located in the Nankai Trough subduction zone, central Japan (Bird 2003; Argus et al. 2011). The Nankai trough subduction zone is well known for repeated M 8 class megathrust earthquakes, which have occurred at intervals of

*Correspondence: yamamotoy@jamstec.go.jp

[1] Japan Agency for Marine-Earth Science and Technology, 3173-25 Showa-machi, Kanazawa-ku, Yokohama, Kanagawa 236-0001, Japan
Full list of author information is available at the end of the article

100–150 years (Ando 1975) (Fig. 1). Nearly 75 years have passed since the most recent events, the 1944 Tonankai (Mw 8.1) and 1946 Nankaido (Mw 8.3) earthquakes. The Japanese government has stated that the possibility for the occurrence of $M > 8$–9 class earthquake within 30 years is as high as 70–80% (The Headquarters for Earthquake Research Promotion 2022). As a result, various seismological and geodetic studies have been conducted on the Nankai Trough subduction zone: For example, a number of these studies demonstrated the subsurface structural heterogeneities that can control rupture propagation (Kodaira et al. 2002, 2006) (Fig. 1)

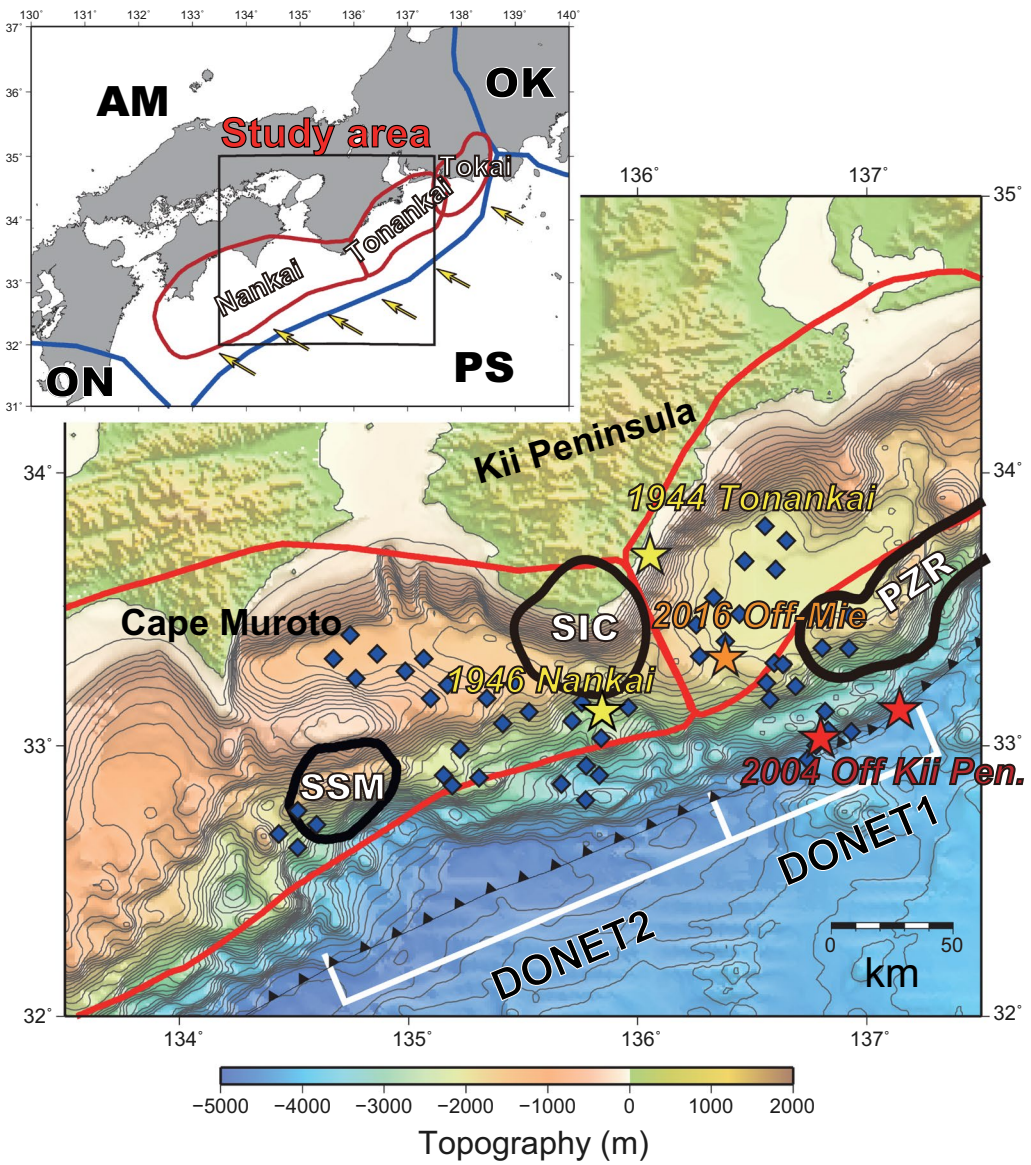


**Fig. 1** Maps of the study area. The inset regional map shows the location of the study area with the megathrust seismogenic segments (Tokai, Tonankai, and Nankai) of the Nankai Trough in southwestern Japan with plate boundaries. Two letter abbreviations reflect the name of the Plate; AM: Amur Plate, PS: Philippine Sea Plate, OK: Okhotsk Plate, and ON: Okinawa Plate (Bird 2003). Yellow allows are the relative motion of the PS with AM (Argus et al. 2011). In the main topographic map, the megathrust seismogenic zones along the Nankai subduction zone are shown by the red line. The Shionomisaki igneous complex (SIC; Kodaira et al. 2006), subducted seamount identified off Cape Muroto (SSM; Yamamoto et al. 2017), and subducted Paleo-Zenith Ridge (PZR; Park et al. 2004) are outlined in black. Blue diamonds show the location of the seismic stations of the Dense Oceanfloor Network system for Earthquakes and Tsunamis (DONET). The epicenters of the 1944 Tonankai and 1946 Nankai earthquakes were taken from Kanamori (1972) (yellow stars), and two M > 7 earthquakes of the Kii Peninsula occurring on September 5, 2004 (red stars) and the $M_{JMA}$ 6.5 off-Mie earthquake occurring on April 1, 2016 (orange star) are from the JMA unified catalog

and indicated the location of the strong coupling regions (e.g., Yokota et al. 2016; Nishimura et al. 2018; Noda et al. 2018).

Moreover, various types of slow earthquakes, long-term and short-term slow-slip events (SSE), very-low-frequency earthquakes (VLFE), tremors, and low-frequency earthquakes have been identified in both the downdip and updip sides of the Nankai Trough seismogenic zone (Obara 2002; Ito et al. 2007; Obara and Kato 2016; Nakano et al. 2018a). The spatiotemporal variation of slow earthquake activity can be expressed as an index of the stress perturbation around the seismogenic zone. For instance, simulation studies have shown that the intervals between the occurrence of slow-slip events along the downdip side of the seismogenic zone are shortened once the onset of a large earthquake approaches (Matsuzawa et al. 2010). Thus, slow earthquakes are being thoroughly monitored to estimate the status and future temporal evolution of the stick–slip behaviors of the Nankai seismogenic zone by the Japan Meteorological Agency (JMA).

It is essential to monitor the spatiotemporal distribution of both slow earthquakes and regular interplate earthquakes for determining the occurrence processes of large earthquakes. However, studies on regular earthquake activity are rare because of their low activity level. Moreover, the accurate determination of the hypocenter location is hampered by the offshore conditions. Unlike the Japan and Ryukyu Trench forearcs, small repeating earthquakes along the plate interface are also inactive in the Nankai Trough forearc (Igarashi 2020). On the one hand, previous offshore seismic observation studies indicated that most of the earthquakes in the Nankai forearc are intraplate events, located within the Philippine Sea slab or overriding Amur Plate (Mochizuki et al. 2010; Yamamoto et al. 2017). On the other hand, based on the offshore seismic observation data, the Mw 5.9 ($M_{JMA}$ 6.5) off-Mie earthquake, which occurred on April 1, 2016, was classified as an interplate earthquake (Nakano et al. 2018b) (Fig. 1). The occurrence of this event indicated the existence of other interplate microearthquakes that could not be detected or have been plagued by in-precise location detection by onshore seismic observation.

From 2010, the Dense Oceanfloor Network system for Earthquakes and Tsunamis (DONET1 and 2; Kawaguchi et al. 2015; Kaneda et al. 2015) was started to establish (Fig. 1). DONET1 and DONET2 have been fully operational since 2012 and 2015, respectively. Broadband seismometers were installed at 51 stations in total, based on which continuous seismic records were obtained. These instruments exhibit superior detection capabilities compared with the land-based observation network. Moreover, offshore observation data can improve the accuracy in epicenter location. However, it remains crucial to identify the effect of velocity structure heterogeneity for accurate epicenter determination. Although previous amphibious seismic tomography based on the offshore temporal seismic observation and active source survey established a three-dimensional (3-D) velocity structure model in this region (Yamamoto et al. 2017), they used only a limited portion of DONET1 stations (Fig. 2a). A recent amphibious tomographic study based on large datasets of both active and passive sources also established a 3-D velocity structure for the entire Nankai Trough seismogenic zone (Arnulf et al. 2022), but they analyzed only P-wave structures and used no offshore seismic stations for passive source data.

Thus, the main aim of this study was to investigate the seismic activity of interplate earthquakes by using seismic data from the DONET. To achieve high accuracy of the estimated hypocenter location, we performed seismic tomography by adding DONET data (Fig. 2b) to a previous 3-D tomographic study (Yamamoto et al. 2017) and updated the velocity structure and hypocenter location simultaneously. Then, we discussed the spatiotemporal patterns of microseismicity around the plate boundary and their relationship with the areal extent of structural heterogeneities, interplate coupling, and slow earthquakes.

## 2 Methods

We established the dataset for seismic tomography in this study by combining data from Yamamoto et al. (2017) with the additional first-arrival data of microseismicity obtained by DONET. We extracted 1999 relocated events and 465 seismic stations as the initial passive source data from Yamamoto et al. (2017) (Fig. 2a). P-wave arrival-time data from previous 11,168 active-source shots along 13 lines at 545 stations were also used. Following the methods of Yamamoto et al. (2017), we used the time difference between S- and P-wave arrivals as input data for two of our ocean bottom seismographs in the off Kumano region that could not be calibrated with Global Navigation Satellite System clock information.

For additional data, we first detected the event by using the STA/LTA method (the ratio between short-time average and long-time average of the waveform amplitude). Both the WIN system (Urabe and Tsukada 1992) and the method of Horiuchi et al. (2009) were applied for all DONET stations (Fig. 2b). Second, we combined these results and deleted duplicates. We manually picked first-arrival times of the detected events on the continuous seismic records at both selected land and all DONET stations. Owing to the processing, the dataset for events occurring from September 2015 to March 2016 and after April 2019 was incomplete and partially analyzed. As a

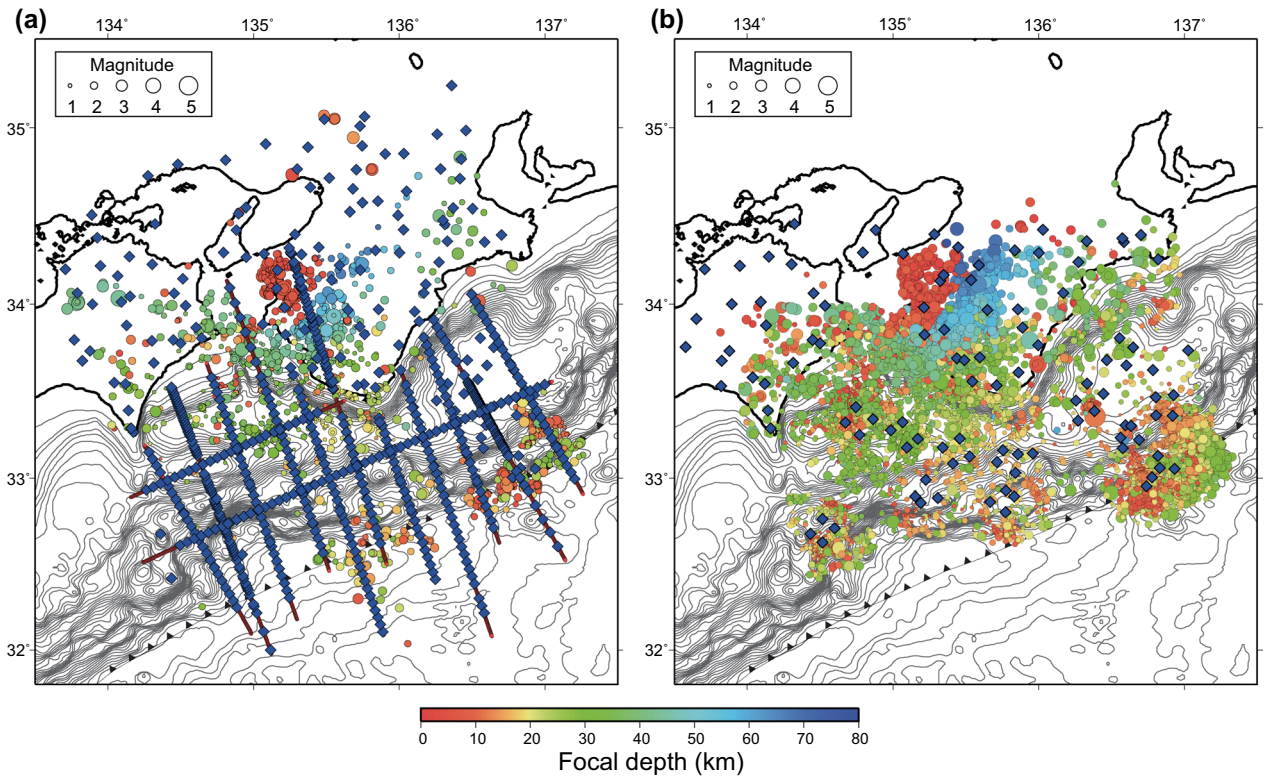


**Fig. 2** Distribution of seismic stations and initial hypocenters. Blue diamonds and colored circle reflect the seismic stations and epicenters, respectively. **a** Selected dataset from Yamamoto et al. (2017). **b** Additional data in this study

result, we detected 21,368 events in total from May 2012 to February 2020. Note that the magnitude for each event was quantified by the using maximum amplitude of a vertical component seismogram (Watanabe 1971).

Then, we conducted hypocenter relocation using the 3-D velocity structure of Yamamoto et al. (2017) to identify the initial location of an additional dataset for tomographic analysis. This procedure was conducted by using the tomoFDD code (Zhang and Thurber 2006). For S-wave first arrivals of the additional dataset, we added a station correction ($\Delta T_S$), calculated from the travel-time differences between the P-to-S converted phases at the basement of the sediment layer and direct P-waves ($T_{PS\text{-}P}$). This procedure was based on Yamamoto et al. (2017).

At the next step, we selected the dataset analyzed in this study using the same criteria from Yamamoto et al. (2017): (1) At least six first-arrival times of P- or S-waves existed, and (2) either a gap in azimuthal coverage was < 180 degrees or the minimum epicentral distance to the nearest station with phase picking was < 30 km. Overall, we obtained 16,042 additional earthquakes for use in the tomographic study (Fig. 2b). As a result, we used a total of 11,168 active source and 18,041 earthquakes at 715 stations (Fig. 3). By utilizing these data, we conducted double-difference seismic tomography. We further applied the tomoFDD package (Zhang and Thurber 2006) and accepted the estimated 3-D velocity model from the previous study (Yamamoto et al. 2017) as an initial 3-D velocity structure. As in a previous study, we set velocity grid nodes at 10 km intervals in the horizontal direction and 2–10 km intervals in the vertical direction. We calculated double-difference data for event pairs whose epicentral distances were < 10 km. As a result, we acquired 423,050 P-wave arrivals, 414,811 S-wave arrivals, 141 S-P intervals, and double-difference data for 2,109,460 P-waves and 1,673,567 S-waves.

We determined the damping parameter for tomographic inversion by considering the recovered amplitudes of a checkerboard resolution test (CRT) (Fig. 4), while the weights and smoothing parameters were established with the same values as in Yamamoto et al. (2017). The sizes of the checkerboard pattern were 20 km, 40 km, and 10–20 km in trough-normal (X-axis), trough-parallel (Y-axis), and vertical directions (Fig. 4f). We assumed that the amplitude of perturbation was ± 3%. We added 0.1 and 0.2 s of Gaussian noise for the P- and S-waves, respectively, to synthetic travel times. We further

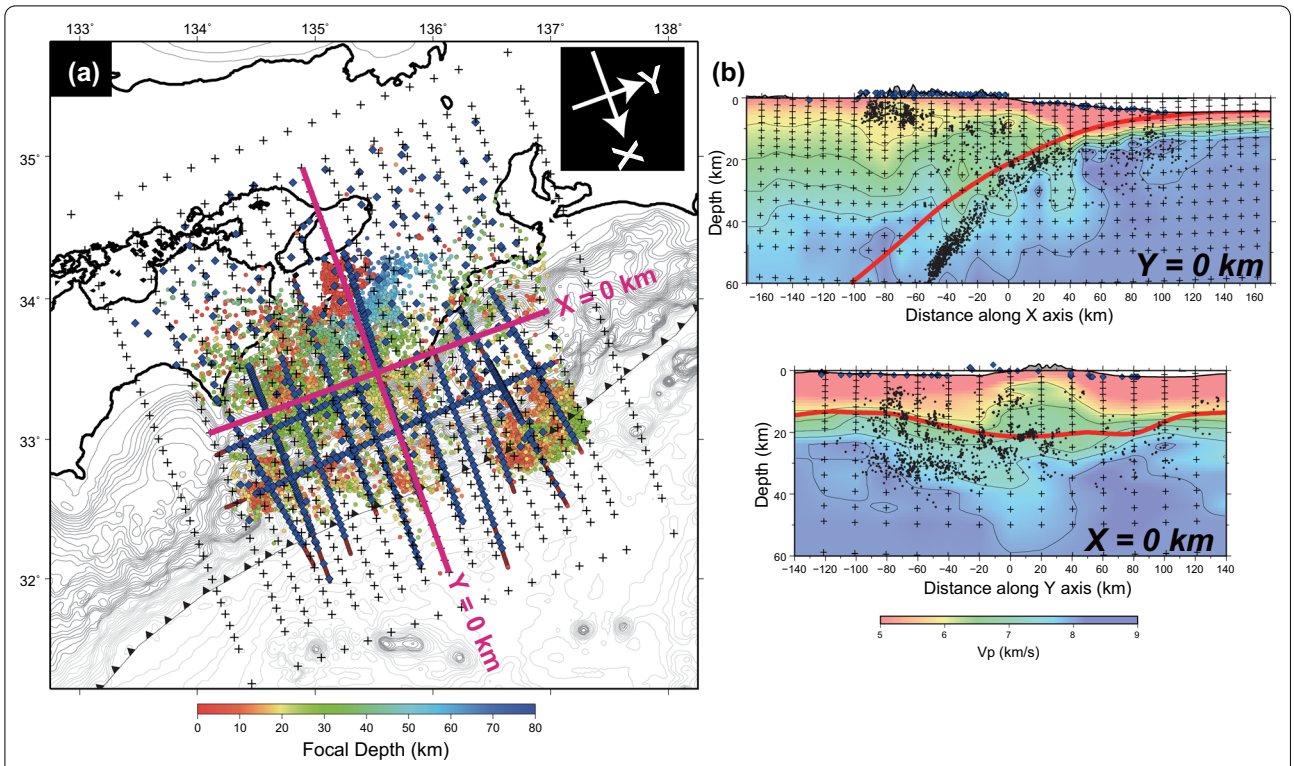


**Fig. 3** Tomographic inversion settings. **a** Crosses, blue diamonds, and colored circles reflect the horizontal distribution of grid nodes for the velocity model, stations, and initial hypocenters, respectively. **b** Initial P-wave velocity model along trough-normal profile at $Y=0$, and along trough-parallel profile at $X=0$ km. Initial hypocenters are shown as black dots. Red line is the plate boundary of Nakanishi et al. (2018). Thin black lines are P-wave velocity contours between 6 and 8 km/s (0.5 km/s increment). Vertical exaggeration = ×2.0

compared the CRT results with the spatial distribution of the derivative weight sum (DWS; Thurber and Eberhart-Phillips 1999), and defined the resolved area based on the following criteria: (1) a recovery rate of CRT, determined by dividing the result of the CRT amplitude by the assumed CRT amplitude, of > 0, and (2) the DWS > 1000 for P-waves and > 500 for S-waves.

## 3 Results

After 10 iterations, the root mean square of the absolute travel-time residuals decreased from 0.28 to 0.22 s for P-wave arrivals and from 0.48 to 0.36 s for S-wave arrivals. As a result, all 18,041 earthquakes were relocated. The average errors of hypocenter relocation were found to be 0.3 km in both the horizontal and vertical directions.

Figure 5 shows the relocated hypocenters. As seen, the offshore earthquakes were distributed to ~40 km depth. To investigate the depth distribution relative to the plate interface, we applied the plate geometry mode of Nakanishi et al (2018). Although there are several other plate geometry models (e.g., Hashimoto et al. 2004; Hirose et al. 2008; Hayes et al. 2018), the model of Nakanishi et al. (2018) included the largest number of offshore seismic surveys; thus, we consider their model to be the most suitable. The result for all the relocated events indicates that most of these events were intraslab events, while the major active areas corresponded to oceanic crust (Fig. 5b). However, most events within the oceanic crust were concentrated within the aftershock region of the 2004 off-Kii earthquake. In addition to the intraslab events, we identified events that occurred close to the plate interface.

Next, we compared our relocation results with the JMA unified catalog (Japan Meteorological Agency 2022). Figure 6a shows both horizontal and vertical differences for $M_{\mathrm{JMA}} > 2$ events. We did not reveal any large differences between our findings and the JMA catalog, despite several events exhibiting ~10 km difference. However, the offshore relocated hypocenters were generally 10–15 km shallower than the focal depths of the JMA catalog. These findings are similar to the trends reported for the aftershock of 2004 off-Kii earthquakes based on offshore seismic observations (Sakai et al. 2005; Nakano et al. 2015). Thus, retrieval of precise focal depth by using only onshore seismic network is hampered. We also compared

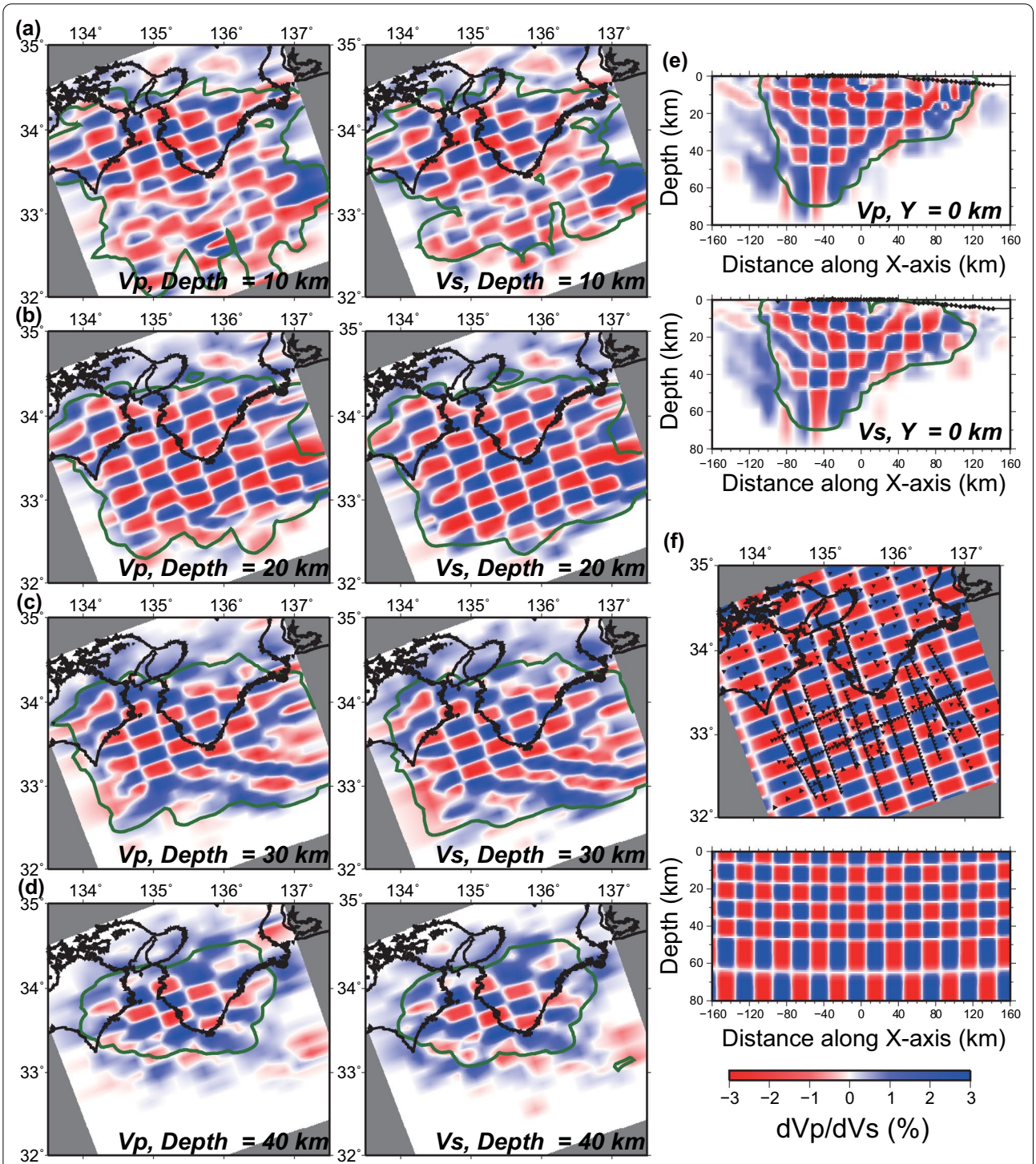


**Fig. 4** Checkerboard resolution test results. **a** At 10 km, **b** 20 km, **c** 30 km, and **d** 40 km depth and **e** along the vertical profile at $Y = 0$ km. Green lines outline areas where the derivative weight sum (Thurber and Eberhart-Phillips 1999) is > 1000 for the P-wave model and > 500 for the S-wave model. **f** Assumed checkerboard patterns

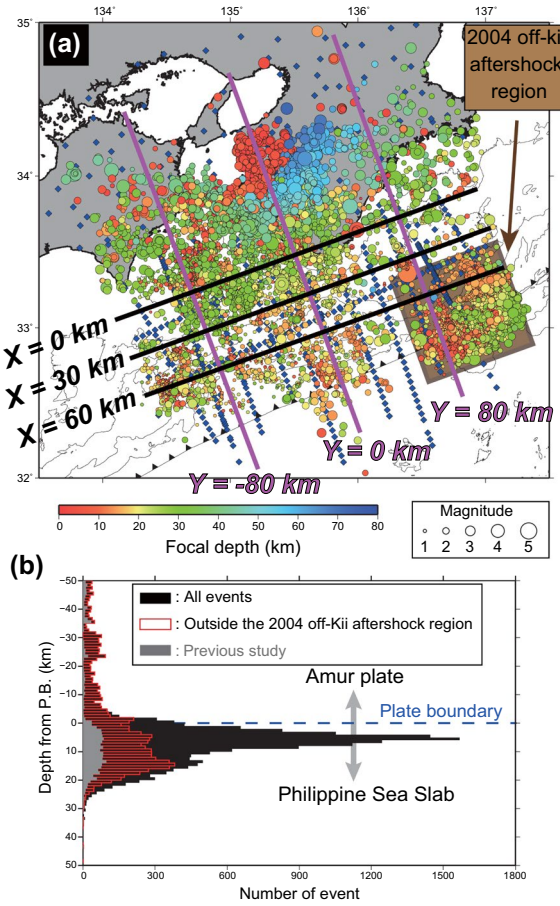


**Fig. 5** Hypocenter relocation results. **a** Map of the relocated hypocenters. Brown rectangle shows the aftershock area of the 2004 off-Kii earthquake. **b** Histogram of the depth distribution regarding the plate boundary model (Nakanishi et al. 2018). Black, red, and gray correspond to all data, outside of the aftershock area denoted in **a**, and from Yamamoto et al. (2017), respectively

the estimated magnitude in this study and that of the JMA (Fig. 6b). Our magnitude was slightly larger than that of the JMA catalog in general. Finally, we examined the distribution of the number of events by magnitude (Fig. 6c). The number of events was evaluated in increments of 0.1, based on the magnitudes from this study. We found that all events above M2.8 were those listed in the JMA catalog, whereas the most of earthquakes whose magnitude was < 2 were not. Thus, the detection capability was strongly improved by the offshore observation.

The estimated velocity model clearly illustrates the subducted Philippine Sea plate down to 40 km depth (Fig. 7). The comparison of these results with the plate interface model of Nakanishi et al (2018) revealed the high velocity slab mantle (Vp > 8.0 km/s, Vs > 4.5 km/s) at ~ 10 km deeper than the plate interface. Moreover, several low-velocity anomaly zones within the slab were identified. The most significant zone was related to the Nankai segment (gray arrow in Fig. 7a; $Y = -80$ km, $X = 20$–$50$ km) for both the P- and S-wave models. We also found that the high-velocity zone just above the plate interface around the toe of the Kii Peninsula (blue arrow in Fig. 7b, $X = 0$ km, $Y = -20$ to 50 km; $X = 30$ km, $Y = -10$ to 30 km).

The analysis of the velocity structure along the plate boundary (Fig. 8) revealed that the Vp = 5 km/s and Vs = 3 km/s iso-velocity contours were nearly parallel to the trough axis. However, larger iso-velocity contours (e.g., Vp = 6 km/s; Vs = 3.5 km/s) tended to be convex to the south, centered at the tip of the Kii Peninsula. The earthquakes within 2.5 km of the plate boundary were clustered in several locations and distributed in the area from near the trough axis to ~ 20 km depth at the plate boundary. A high velocity region with Vp > 8 km/s and Vs > 4.25 km/s was imaged beneath the Kii Peninsula (34°N,135.5°E), and deep low-frequency tremors (Maeda and Obara 2009; Obara et al. 2010) were distributed on the updip side of this region.

## 4 Discussion

### 4.1 Location and spatial extent of structural anomalies

First, we evaluated how the structural heterogeneities, estimated by previous studies, were reconstructed by our velocity model. In the overriding Amur Plate, high-density and high-seismic velocity body called the Shionomisaki igneous complex (SIC) exists just beneath the toe of the Kii Peninsula (Honda and Kono 2005; Kodaira et al. 2006; Qin et al. 2021). In both the average P- and S-velocity perturbations within a 5-km-thick layer just above the plate interface (Fig. 9a), the high-velocity zone is clearly imaged. In particular, the center of the high-velocity zone (A in Fig. 9a), located just north of the epicenter of the 1946 Nankai earthquake, was attributed to the highest gravity anomaly (Honda and Kono 2005). This finding leads to the conclusion that this high-velocity region represents the spatial extent of the SIC.

Based on the interpretation of Kimura et al (2014), this high-velocity region reaches the vicinity of the wedge mantle. The high-velocity zone between 30 and 40 km of the depth contour of the plate interface (B in Fig. 9a; 34° N, 135.5° E) corresponds to the landward mantle because the depth of Moho discontinuity in this area is shallower than 30 km (Matsubara et al. 2017). Although areas A and B were seemingly separated in the S-wave velocity model, their boundary was unclear in the P-wave velocity model (Fig. 9a). Arnulf et al. (2022) also investigated the spatial extent of SIC (called the "Kumano Pluton" in their paper) based on the high (> 6.5 km/s) P-wave velocity zone. The P-wave velocity contour of 6.5 km/s from our model at 15 km depth (green line in Fig. 10a) and the spatial extent

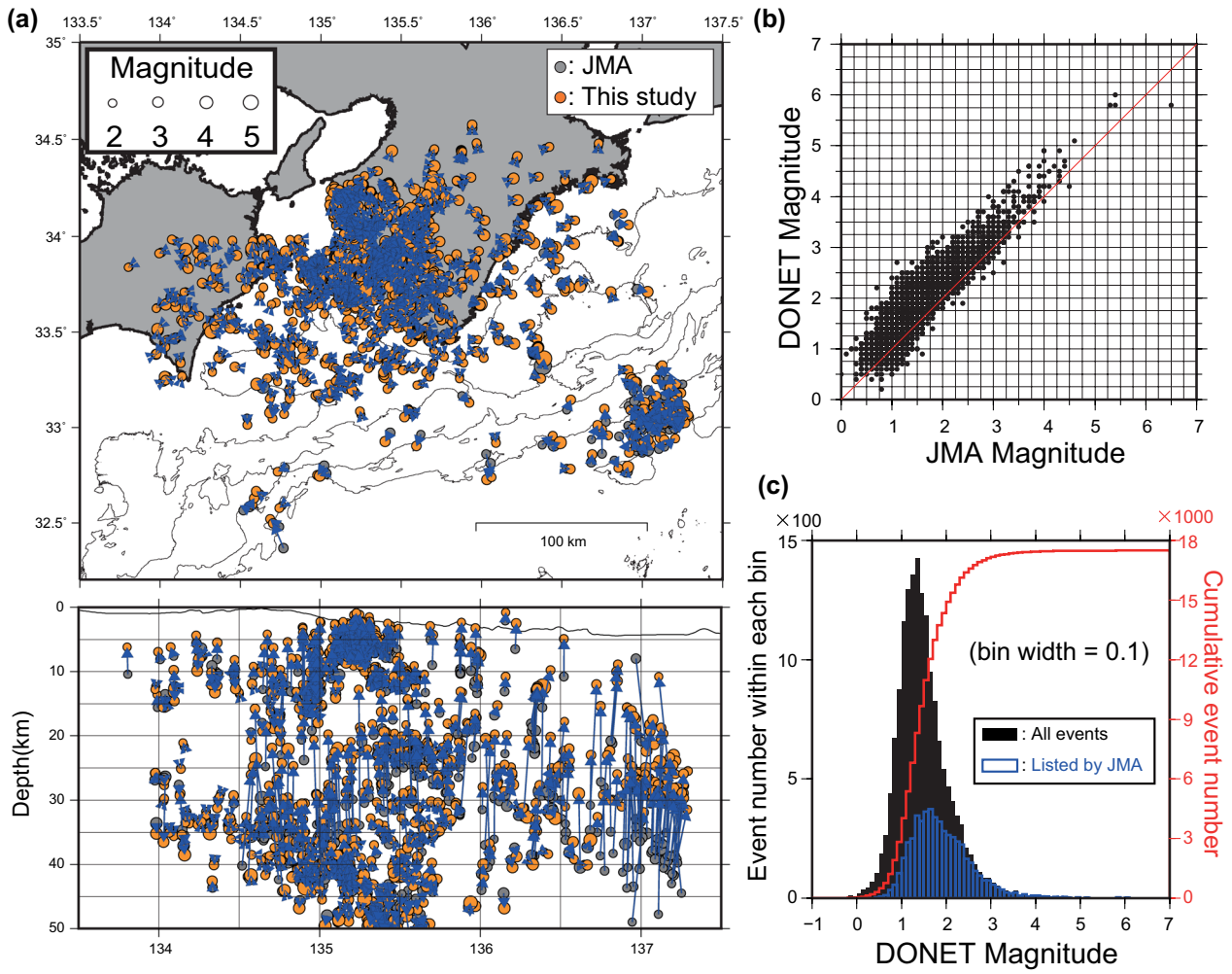


**Fig. 6** Comparison of hypocenter parameters between this study and the JMA unified catalog. **a** Difference in locations. Blue arrows show the vector from the JMA catalog to the relocation result. **b** Difference in magnitude. **c** Histogram reflecting the magnitude distribution. Black and blue bars show the number of events included in each bin whose width is 0.1 for all events and the event listed in JMA catalog, respectively. The red line is the cumulative histogram for all events

of the Vp > 6.5 km/s areas within the overriding plate along Y-axis direction ($-30 \leq X \leq 40$ km; black lines in Fig. 10a) are consistent with their result. Note that the Vp > 6.5 km/s areas of our model located south of the overlapped area with Arnulf et al. (2022) correspond to the oceanic crust of the subducting plate. Based on this consistency, we determined that the southern limit of the SIC was imaged by our model. However, our result is inconsistent with theirs at north of 34° N (Fig. 10a). In addition, it is difficult to estimate the spatial extent of Vp > 6.5 km/s areas along the northern side ($X \leq -40$) owing to the extent of the wedge mantle. Therefore, the north extent of the SIC was not determined in this study.

In certain subduction zones, the relationship between the structural heterogeneity of the upper plate and the seismic slip distribution has been previously investigated, thereby indicating that the high-velocity zone corresponds to the large coseismic slip zone (e.g., Zhao

(See figure on next page.)

**Fig. 7** Obtained velocity model along vertical profiles. **a** Along $Y = 80$ km, 0 km, and $-80$ km, **b** $X = 0$ km, 30 km, and 60 km (locations shown in Fig. 5a). Unresolved areas are masked by gray. White dots and blue diamonds reflect relocated earthquakes and seismic station within 10 km of each profile, respectively. Gray and blue double arrows reflect the location of characteristic structural anomalies. Vertical exaggeration = ×2.0. Other symbols are same as in Fig. 3b

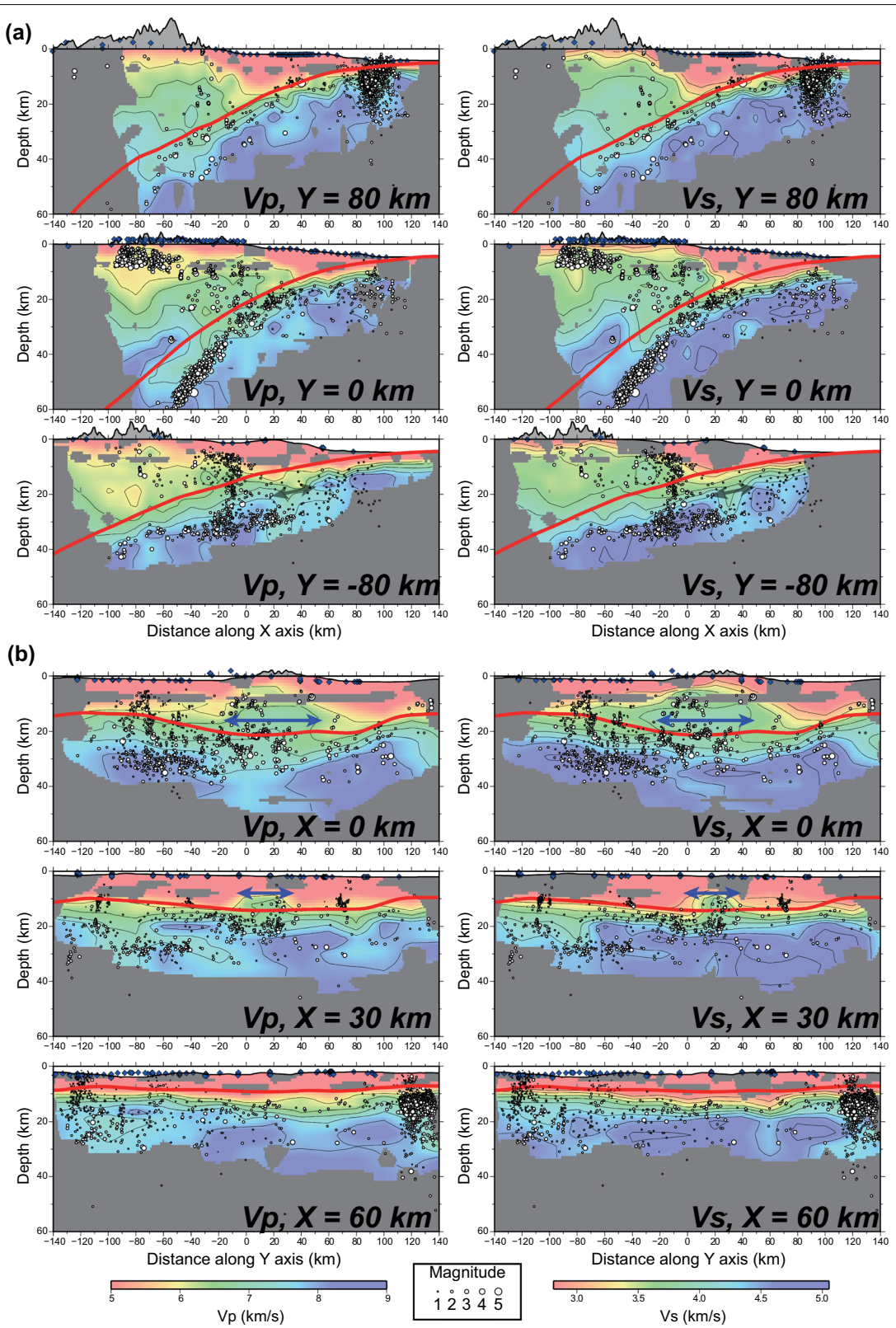


**Fig. 7** (See legend on previous page.)

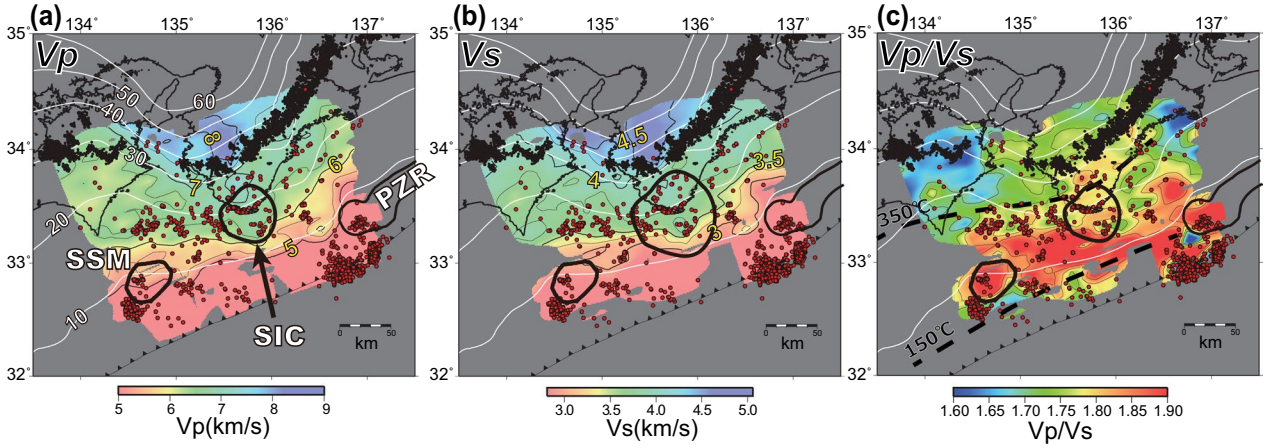


**Fig. 8** The estimated velocity structure along the plate interface. Red and black dots reflect the relocated hypocenters within 2.5 km from the plate interface and the deep low-frequency tremor (Maeda and Obara 2009; Obara et al. 2010), respectively. White contours show the iso-depth of plate interface with a 10 km increment (Nakanishi et al. 2018). **a** P-wave velocity structure. Black lines show the iso-velocity contours from 5 to 8 km/s with 0.5 km/s increments. **b** S-wave velocity structure. Black lines show the iso-velocity contours from 3 to 4.5 km/s with 0.25 km/s increments. **c** Vp/Vs structure. Black lines show the iso-value contours from 1.7 to 1.9 with 0.1 increments. Thick dashed lines correspond to the isotherm contour for 150 and 350 °C (Oleskevich et al. 1999). Other symbols are the same as Fig. 1a

et al. 2011). For the area of interest in this study, we compared the structure with the distribution of interplate coupling strength (Yokota et al. 2016) and did not find a significant relationship, thereby agreeing with Yamamoto et al. (2017). Note there are various models for the slip distribution of the 1944 Tonankai and 1946 Nankai earthquakes whose characteristics were not similar. For example, the largest slip areas of the 1946 Nankai earthquake in Baba and Cummins (2005) do not overlap with those reported by Murotani et al. (2015). Thus, the comparison between our velocity structure and the slip distribution of past megathrusts was not conducted in this study.

Within the slab, the existence of subducted topographic anomalies, such as seamounts (Kodaira et al. 2000) and the Paleo-Zenith Ridge (Park et al. 2004), has been previously reported. We attempted to identify their location from our velocity model. As these features are characterized by thick crust, they are illustrated as low-velocity regions in the deep structure of the slab relative to the surrounding mantle. Figure 9b shows the average velocity perturbation within a 5-km-thick layer between 10 and 15 km beneath the plate interface. We identified two low-velocity zones (C and D in Fig. 9b). Here, low-velocity zone C corresponded to the subducted seamount (Kodaira et al. 2000), and its spatial extent was nearly the same as that from Yamamoto et al. (2017). Low-velocity zone D was located close to the area where the Paleo-Zenith Ridge subducted (Park et al. 2004), thereby indicating no overlap with the resolved area from Yamamoto et al. (2017). Although the location of low-velocity zone D from P-wave perturbations was slightly south of that of the S-wave perturbations, this low-velocity zone was attributed to the existence of the Paleo-Zenith Ridge. Although smaller-size subducted seamounts than our grid spacing can theoretically exist, we could not find other similar low-velocity zones in the study area. Thus, it is reasonable to suggest that there was seemingly no other subducted seamount or ridge as large as them.

Arnulf et al. (2022) observe a significant (Vp = 6.5–7.5 km/s) low-velocity anomaly within the subducting mantle around the aftershock region of the 2004 off-Kii earthquake and interpreted it as a combination of serpentinization and enhanced porosity from bending stress. Although their model has the lowest point of P-wave velocity at 30 km depth, there is no such low-velocity zone in our model (Fig. 10b). Note that the low-velocity zones imaged between the 20 and 30 km contour of the plate interface depth correspond to the oceanic crust. Instead, the location of the significant low P-wave area (Vp < 6.5 km/s) from their model was spatially close to the subducted Paleo-Zenith Ridge, where we found the low-velocity anomaly 10–15 km beneath the plate interface (Fig. 9b). That is, the depth of the low-velocity anomaly obtained in our study was ~ 10 km shallower than that of Arnulf et al. (2022). We consider this difference to be due to the poor hypocenter location accuracy in the dataset of Arnulf et al. (2022). As shown in Fig. 6, there is a large difference in hypocenter depth of offshore seismicity between this study and the JMA unified catalog, which Arnulf et al. (2022) applied. Because their analysis was performed by earthquakes whose calculated depths were

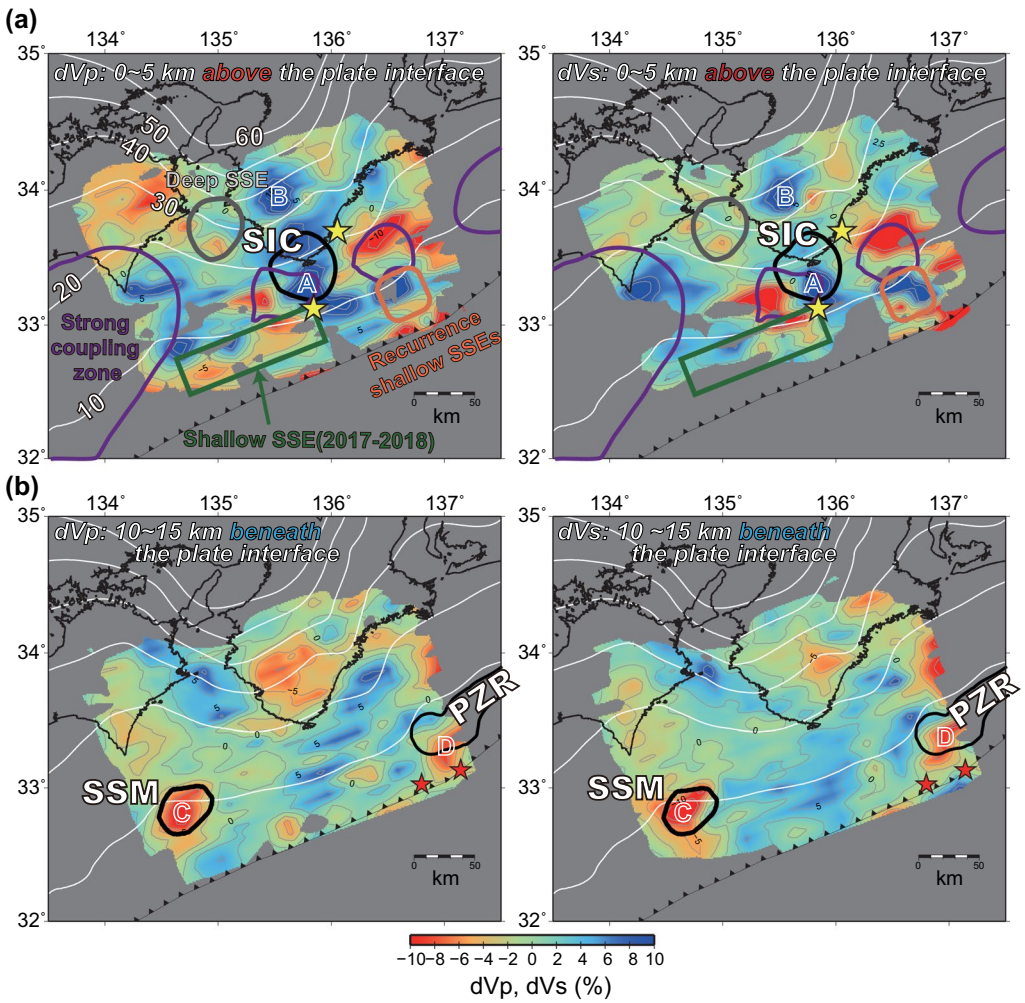


**Fig. 9** Velocity perturbation within the 5-km-thick layer. **a** At just above the plate interface and **b** between 10 and 15 km below the plate interface. White contours are depth to the plate boundary (Nakanishi et al. 2018). Dashed contours reflect velocity differences from − 10 to + 10% at 2.5% increments. The areas of strong (> 5 cm/year) interplate coupling estimated from onshore and offshore geodetic data are outlined by purple lines (Yokota et al. 2016). Areas outlined by gray, green, and orange lines reflect the fault location of deep SSE beneath the Kii channel (Kobayashi 2014), shallow SSE between 2017 and 2018 (Yokota and Ishikawa 2020), and recurrence shallow SSE (Araki et al. 2017; Ariyoshi et al. 2021), respectively. A, B, C, and D are the locations of substantial velocity anomalies discussed in the main text. Other symbols are the same as in Fig. 1

more than 10 km deeper than their actual depth, the low-velocity region shown in Arnulf et al. (2022) was imaged at a deeper position than the actual location.

### 4.2 Spatial relationship among interplate earthquakes, interplate coupling, and slow earthquakes

We confirmed the occurrence of interplate earthquakes in the study area (Fig. 8). The comparison with the thermal structure (Oleskevich et al. 1999) revealed that most interplate earthquakes occurred between 150 and 350 °C, thereby resonating with the range of seismogenic zone depth (Hyndman et al. 1997). In addition, they were seemingly located outside of high Vp/Vs (> 1.9) zone except for two areas, where a subducted topographic high was identified (Fig. 8c). The downdip limit of the Vp/Vs > 1.9 zone was located ~ 100 km from the trough axis in line with the downdip limit of the dehydration occurred within the sediment layer (Hyndman and Peacock 2003). The high Vp/Vs ratio around the plate interface normally indicates the existence of pore fluids and is attributed to the weak coupling zone as pore fluids decrease the effective normal stress (Moreno et al. 2014). Thus, interplate seismicity can be interpreted as occurring in areas with relatively less pore fluid and not fully creeping zones. However, the high Vp/Vs zone in this study area contained at least one strong interplate

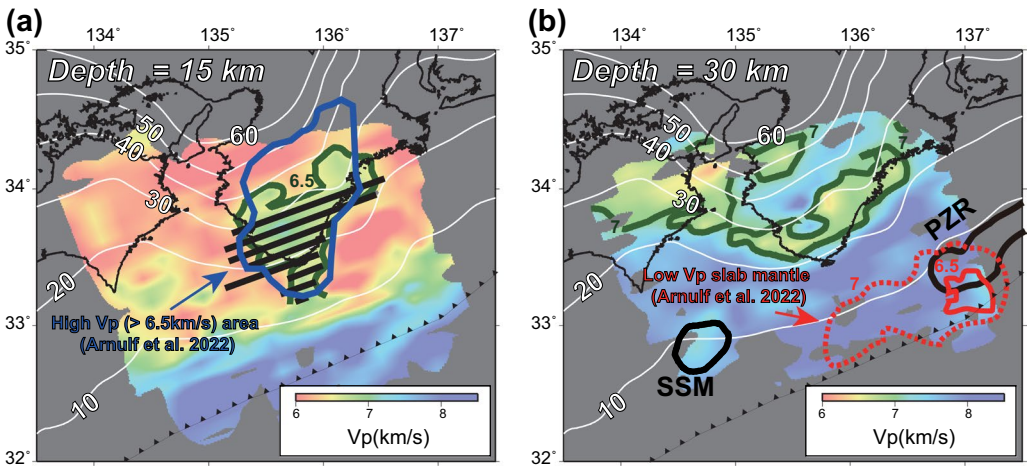


**Fig. 10** P-wave structure along the depth slice. **a** At 15 km depth. The green line is the iso-value contour of Vp = 6.5 km/s in our model. Black lines show the spatial extent of Vp > 6.5 km/s along the *Y* direction ($-30 \leq X \leq 40$ km). The blue line shows the high velocity zone estimated by Arnulf et al. (2022). **b** At 30 km depth. The green line is the iso-value contour of Vp = 7.0 km/s in our model. The red solid and dotted lines show the Vp contours of 6.5 km/s and 7.0 km/s 15 km deeper than slab Moho discontinuity estimated by Arnulf et al. (2022), respectively

coupling area (Yokota et al. 2016), indicating that the relationship between Vp/Vs and coupling strength along the plate boundary proposed by Moreno et al. (2014) cannot be applied to the Nankai Trough. Thus, the existence of interplate microearthquakes cannot be simply attributed to the Vp/Vs distribution. Rather, there are other potential factors, such as topographic anomalies in the subducted plate (Nakamura et al. 2022) or thickness variation of the subducted sediment layer (Akuhara et al. 2017), that may control the occurrence of interplate seismicity in the Nankai trough.

To identify the areas where interplate earthquakes prevailed, we selected the earthquakes within 1 km of the plate interface (Nakanishi et al. 2018). On this basis, we defined 14 areas as active areas of interplate earthquakes (Fig. 11). These active areas were generally located outside the especially strong coupling zones (>5 cm/yr; Yokota et al. 2016), except Area 11, where the Mw 5.9 off-Mie earthquake occurred on April 1, 2016 (Nakano et al. 2018b) (Fig. 11a). Two areas in the vicinity of the trough axis (Areas 13 and 14) corresponded to the aftershock area of the 2004 off southeastern Kii earthquakes.

At the next step, we examined the relationship between these 14 active areas and slow earthquakes. We did not find overlap with the SSE region in the Kii Channel (Kobayashi 2014). The segregation of slow earthquakes and regular earthquakes at the plate boundary has been previously demonstrated in the off Boso (Ito et al. 2019), Ryukyu Trench (Yamamoto et al. 2018; 2020), Hikurangi (Bartlow et al. 2014), and other areas. However, in the offshore, there was an area of overlap with the fault location of the SSE between 2017 and 2018 (Yokota and Ishikawa 2020) (Area 9; Fig. 11a). Moreover, three areas (Areas 8, 9 and 12) corresponded to the area where shallow VLFE was identified based on the offshore observation (Sugioka et al. 2012; Nakano et al. 2018a; Toh et al. 2020; Yamamoto et al. 2022). The overlapping areas were all located at the area, where the plate interface was located at the depth of ~7 km and was attributed to the subduction position of a seamount or its vicinity (Fig. 11a). The source location accuracy of VLFE was found to be lower (e.g., ~0.03° in horizontal and 1.3 km in depth for VLFE in Yamamoto et al. 2022) than that of the relocated hypocenters in this study (~0.3 km in both the horizontal and vertical direction in this study). Thus, a fine-scale analysis is challenging with the current methodology, but it is reasonable to suggest that several of the active areas of interplate earthquakes in the Nankai Trough subduction zone overlapped with the source areas of the slow earthquakes. Compared with the estimation of the VLFE location based on onshore data (Takemura et al. 2019), the active areas in Areas 6, 7, and 13 seemingly overlapped with VLFE (Fig. 11b). However, as the VLFE location, estimated by Takemura et al. (2019), was plagued by large uncertainty in the across-trough direction (see Fig. S1 of Takemura et al. 2019), their result may not reveal spatial differences between Areas 6 and 8, Areas 7 and 9, and Areas 12 and 13.

Both slow earthquakes and microearthquakes along the fault have been previously thought to occur in the transition zone between the strong coupling seismogenic zone and fully creeping zone (e.g., Sholtz 2002; Obara and Kato 2016). The magnitude of completeness for microearthquakes in this study is less than 2 (Fig. 6), which is much lower than that for VLFE (~Mw = 3; Nakano et al. 2018a, b;

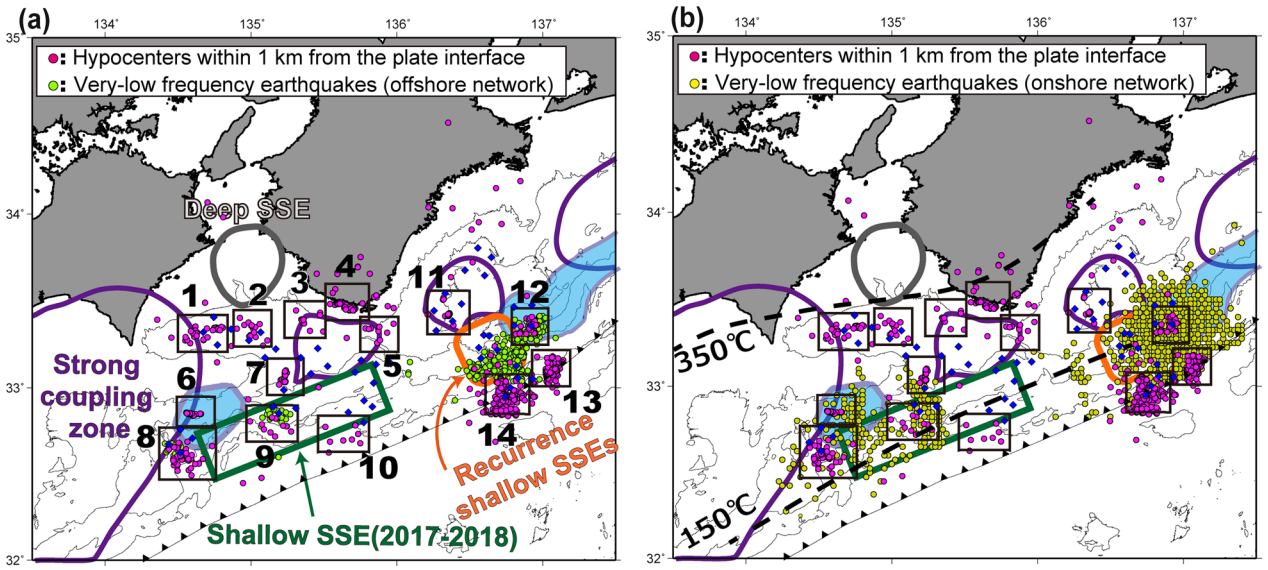


**Fig. 11** The location of the active areas for interplate seismicity and very-low-frequency earthquakes (VLFEs). Relocated hypocenters within the 1 km from the plate interface are shown by pink circles. **a** Numbers from 1 to 14 reflect area code. VLFEs estimated by using the offshore seismic network are shown by green circles (Sugioka et al. 2012; Nakano et al. 2018a; Toh et al. 2020; Yamamoto et al. 2022). Location of the subducted seamount off Muroto and the Paleo-Zenith Ridge is shown by light-blue areas. **b** VLFEs estimated by using onshore seismic network are shown by yellow circles (Takemura et al. 2019). Other symbols are the same as in Fig. 9

Yamamoto et al. 2022). In addition, the improvement of the accuracy in the hypocenter relocation using the offshore seismic network with a 3-D velocity model enabled the distinction between interplate and intraplate earthquakes. As both the detection capability and location accuracy of regular earthquakes were superior to those of shallow slow earthquakes, a comprehensive detection of interplate microearthquakes is valuable for monitoring the current stick–slip status of the strong coupling zone in the Nankai Trough.

### 4.3 Temporal variation of interplate earthquake activities

For each active zone, we examined the temporal changes in seismic activity and the number of integrated earthquakes at the plate boundary ± 25 km by using the entire relocation result from this study (Fig. 12). Because the network-based observations exhibited temporal variability, we focused on the temporal distribution after March 2015 at the area close to the DONET2 network (Areas 1–10) and after 2012 at the area within the DONET1 network (Areas 11–14), respectively. No remarkable changes were identified in Areas 1–5, which were close to land, or in Areas 10, 13, and 14, which were close to the trough axis. However, in other areas, characteristic activity was identified, even while considering the periods when the dataset was incomplete (gray masked periods in Fig. 12).

In Areas 6, 8, and 9, the cumulative number of earthquakes increased sharply in 2018. Seafloor crustal displacement observations in this area suggest that SSEs occurred between 2017 and 2018 (Yokota and Ishikawa 2020). As the activations in these areas during the SSE period seemingly occurred between − 5 and 5 km in relative depth (Fig. 12), we examined the temporal variation of five areas close to this SSE region. Therefore, we narrowed the time window to two years and the epicenter to ± 5 km from the plate interface (Fig. 13a). As a result, swarm-like activation of interplate seismicity in Areas 8 and 9 was identified in March and May 2018, respectively.

(See figure on next page.)

**Fig. 12** Temporal variations of seismicity in each area shown in Fig. 11. Blue dots reflect relocated hypocenters, and their vertical axis is relative depth from the plate interface. The red line shows the cumulative number of earthquakes within the relative depth range between − 25 and 25 km. Operation periods for each seismic observation are shown on the upper side of the panel by colored arrows; OBS1,2: ocean bottom observation data from Yamamoto et al. (2017), DONET1, and DONET2. Masked areas of gray, green, and orange reflect the period of incomplete dataset, shallow slow-slip events (SSEs) estimated by Yokota and Ishikawa (2020), and recurrence SSEs (Ariyoshi et al. 2021), respectively. The pink triangle with dotted line reflects the timing of the April 1, 2016, Mw 5.9 earthquake

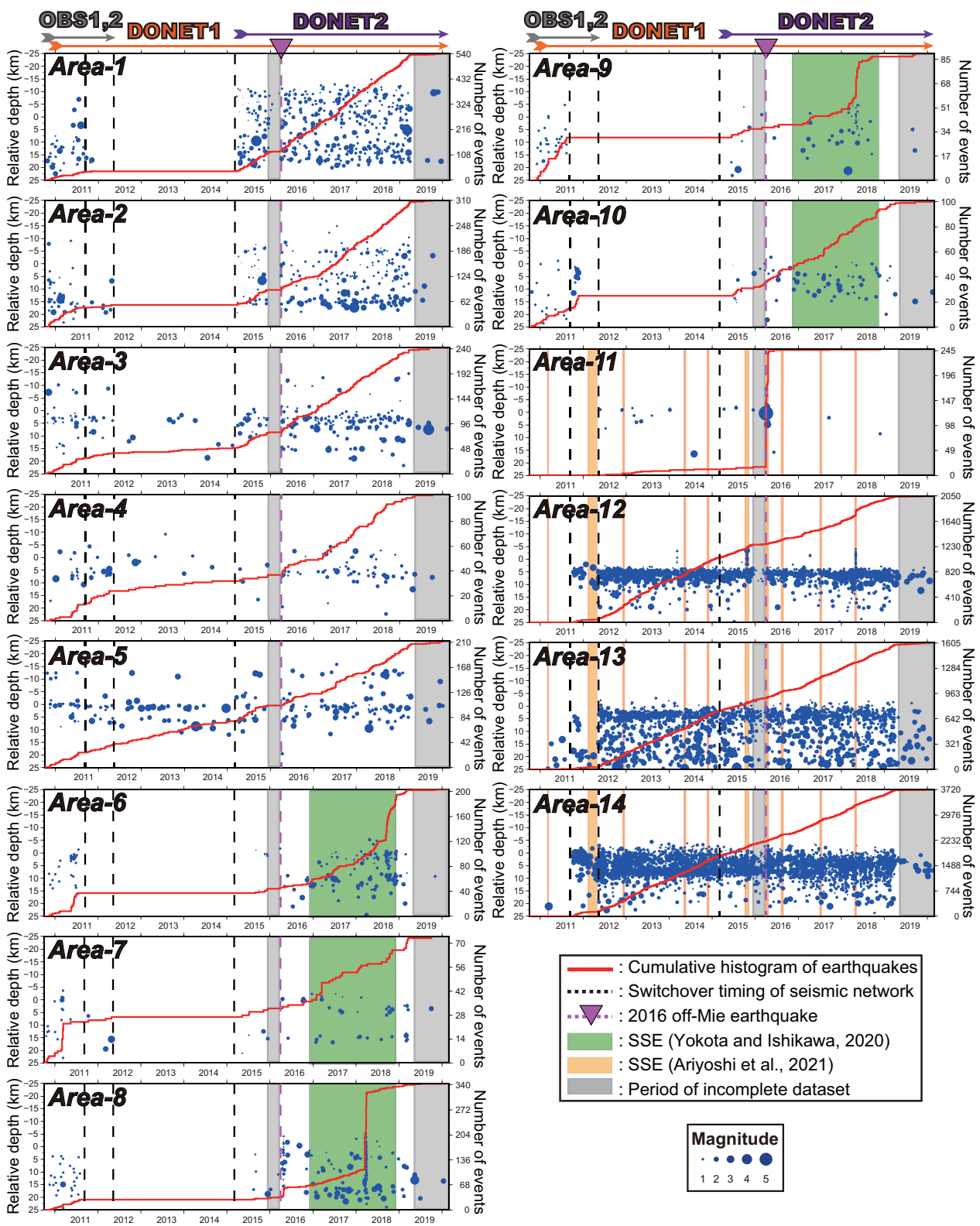


**Fig. 12** (See legend on previous page.)

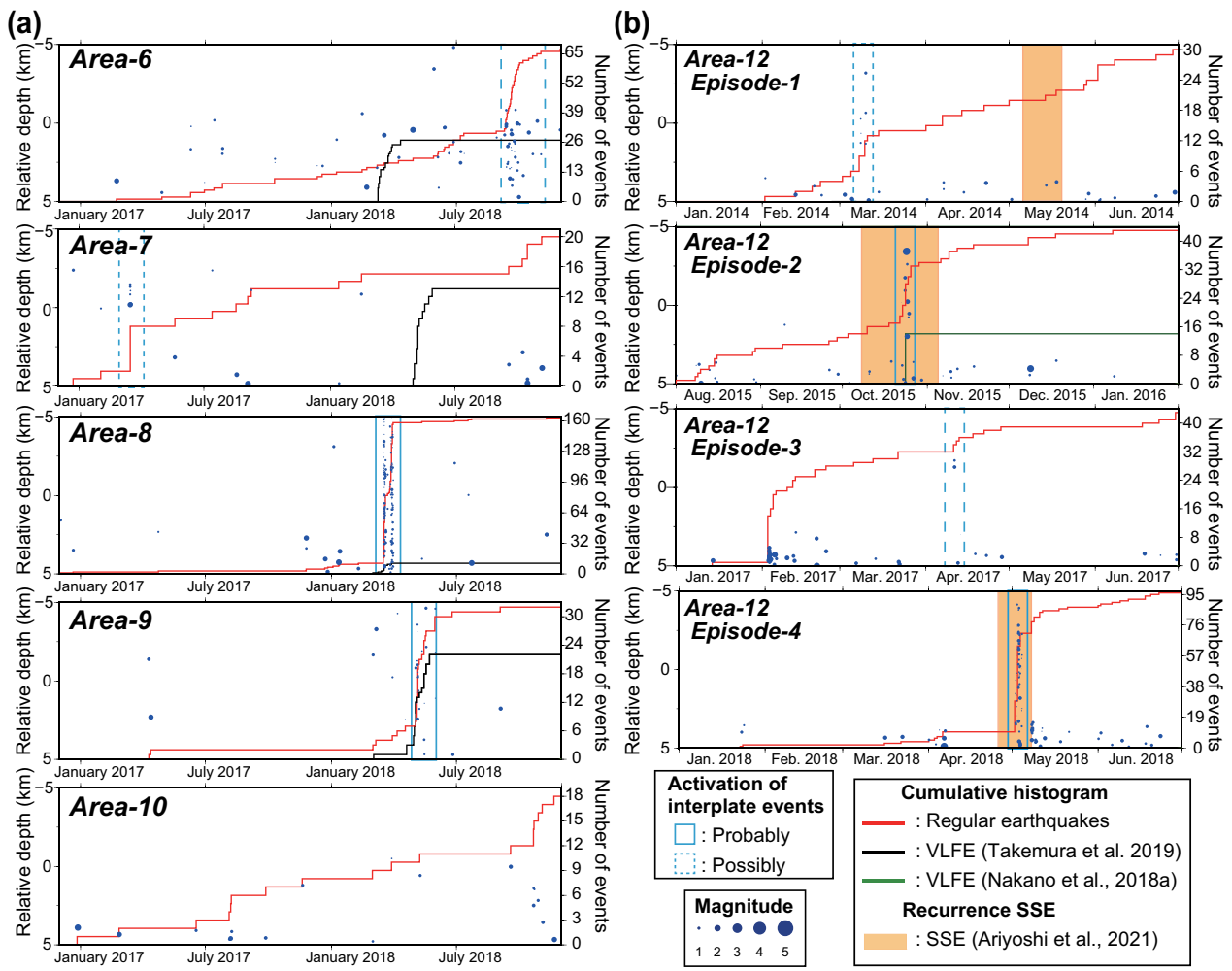


**Fig. 13** Temporal variation of seismicity within 5 km from the plate interface. **a** In Areas 6 to 10 during shallow slow-slip event occurrence (time window is 2 years), **b** in Area 12 around the time when swarm-like activity was observed (time window is 6 months). The black line in **a** and green line in **b** are the cumulative number of VLFEs reported by Takemura et al. (2019) and Nakano et al. (2018a), respectively. Light-blue boxes reflect the confirmed activation of interplate seismicity as read visually; dotted boxes are less clear than the solid boxes. Other symbols are the same as in Fig. 12

Although detailed discussion is not possible owing to the lack of an available VLFE catalog from offshore observation corresponding to this SSE, VLFE activity has been previously reported by Takemura et al. (2019), with most activity near the western side (Area 8) in March and the eastern side (Area 9) in May (black line in Fig. 13a).

However, the activation of interplate seismicity seen in Area 6 occurred approximately six months later than the timing of the VLFE activity observed by Takemura et al. (2019). Moreover, VLFE activity was not accompanied by the interplate seismicity in Area 7, and no swarm-like seismicity or VLFE activity was identified in Area 10. The onshore network-based VLFE activity periods were the same between Areas 6 and 8 and between Areas 7 and 9. This finding might indicate the previously indicated large location uncertainty in across-trough direction. Thu, it is necessary to determine the source locations of the VLFE by using the seafloor observation network during this activity period to determine the difference in activity between regular earthquakes and VLFE and to understand the state of stick–slip behavior in the shallow part of the subduction zone.

In Area 11, a sharp increase in the cumulative number of earthquakes related to the 2016 off-Mie earthquake was identified (Fig. 12). Unlike the other areas, this area was located within the strongly coupled zone (Yokota et al. 2016), where we also observed several seismic

activities occurring near the plate boundary before the 2016 earthquake (e.g., in 2013 and 2015). This indicates that the 2016 off-Mie earthquake did not occur at the seismic gap but in an area of background seismicity. The investigation of the location of background interplate seismicity within the strongly coupled area can unravel a potential nucleation point for moderate-size or, even large interplate earthquakes.

Area 12 seemingly had no significant fluctuations during this period, except a slight increase in the cumulative number of earthquakes in the first half of 2018 (Fig. 12). However, a deeper investigation of Area 12 suggests that while intraslab earthquakes (>5 km deeper than plate interface) generally prevail, earthquakes occur at relatively shallow depths close to the plate boundary (within 5 km from the plate interface) in four episodes during the observation period: the first half of 2014 (episode-1), the second half of 2015 (episode-2), the first half of 2017 (episode-3), and the first half of 2018 (episode 4) (Fig. 13b). The first and third episodes exhibited fewer earthquakes, while the second and fourth episodes experienced more earthquakes. Based on borehole pore pressure changes, recurrent SSEs were shown to occur in the area adjacent to the western region (Araki et al. 2017; Ariyoshi et al. 2021) (Fig. 11a). Of these events, SSEs with large amounts of slip were reported during episodes 2 and 4. VLFE activity was also confirmed by the offshore observation data during episode 2 (Nakano et al. 2018a), although no VLFE was observed during episode 4.

This study proved the existence of interplate earthquake swarms, synchronized with SSEs at Areas 8, 9, and 12 in the Nankai Trough. Such earthquake swarms, associated with SSE, have been previously reported in subduction zones such as off Boso (Hirose et al. 2014; Fukuda 2018), Ecuador (Vaca et al. 2018), and Hikurangi (Bartlow et al. 2014), where slow-slip stress loading and stress triggering outside the SSE region were the main drivers of earthquake swarms. In this study, the seismic swarm activity in Areas 8, 9, and 12 may have been activated by the SSE, because the timing of the SSE and VLFE activity was the same.

Near the subducted seamount in the Hikurangi forearc, similar regular earthquake swarms collocated with slow earthquakes were reported, but they were located within the overriding plate (Shaddox and Schwartz 2019). The observed waveforms near the swarm areas generally indicate an increasing difference between S- and P-wave arrivals with respect to hypocenter depth (Fig. 14). Considering this result and the accuracy of our hypocenter depth in this study (~0.3 km), we suggest that seismic swarms observed in this study are located within the slab and across the upper plate and include seismic activity at the plate boundary, rather than being located solely within the overriding plate as in Hikurangi. The focal mechanisms of low angle thrust solutions should be a strong piece of evidence for interplate seismicity. Although we could estimate the focal mechanism for the 2016 off-Mie earthquake based on P-wave polarity data by applying the FOCMEC package (Snoke 2003) as a low angle thrust (Fig. 14b), focal mechanism solutions could not be obtained for swarm activities collocated with slow earthquakes owing to their small magnitudes. Further study by adding the information of the S-phase waveforms may allow us to estimate a number of their focal mechanisms.

In Area 8, seismic activity swarms occurred twice with an interval of ~10 days (Fig. 13a). This finding suggests that monitoring of seismic swarm activity around the plate boundary may lay the foundation for estimating the state of interplate stick–slip changes with higher temporal resolution. Furthermore, episode 4 in Area 12 (with the largest number of interplate seismic activity but composed of smaller magnitude than that in episode 2) was not accompanied by any VLFE (Fig. 13b). Based on the relationship between the seismic energy release and magnitude (Gutenberg and Richter 1956), the summation of the seismic energy release for the swarm activity during episode 2 was estimated as $2.53 \times 10^8$ N m, much larger than that during episode 4 ($6.77 \times 10^7$ N m), respectively. This, in turn, indicates that the total energy release during swarm activity was one of the indicators of the magnitude of SSEs.

Note that in most previous studies, the SSE areas and seismic swarm activity areas did not spatially overlap but were rather adjacent to each other. In this study, the occurrence of swarm earthquakes within the area of SSE and/or VLFE activity was also confirmed, but large uncertainties were identified in the location of shallow slow earthquakes. Hence, the detection of seismic swarm activity along the plate interface can strengthen the accuracy, thereby improving the estimation of slow-slip fault models. Furthermore, if the number of detections can be increased, as in the case of Nicaragua (Thorwart et al. 2013), one can retrieve physical parameters on the fault, such as diffusion coefficients and porosity based on the swarm seismicity catalog. As the minimum magnitude of the earthquake swarms obtained in this study was very small, compared to previous studies, it is essential to take advantage of the offshore seismic networks. The use of seafloor observation networks and hypocenter determination by using 3-D velocity model should extend the prospects for estimating spatiotemporal changes of b-values focused on the plate interface in the Nankai megathrust seismogenic zone, which has only previously been discussed with regard to spatial changes based on

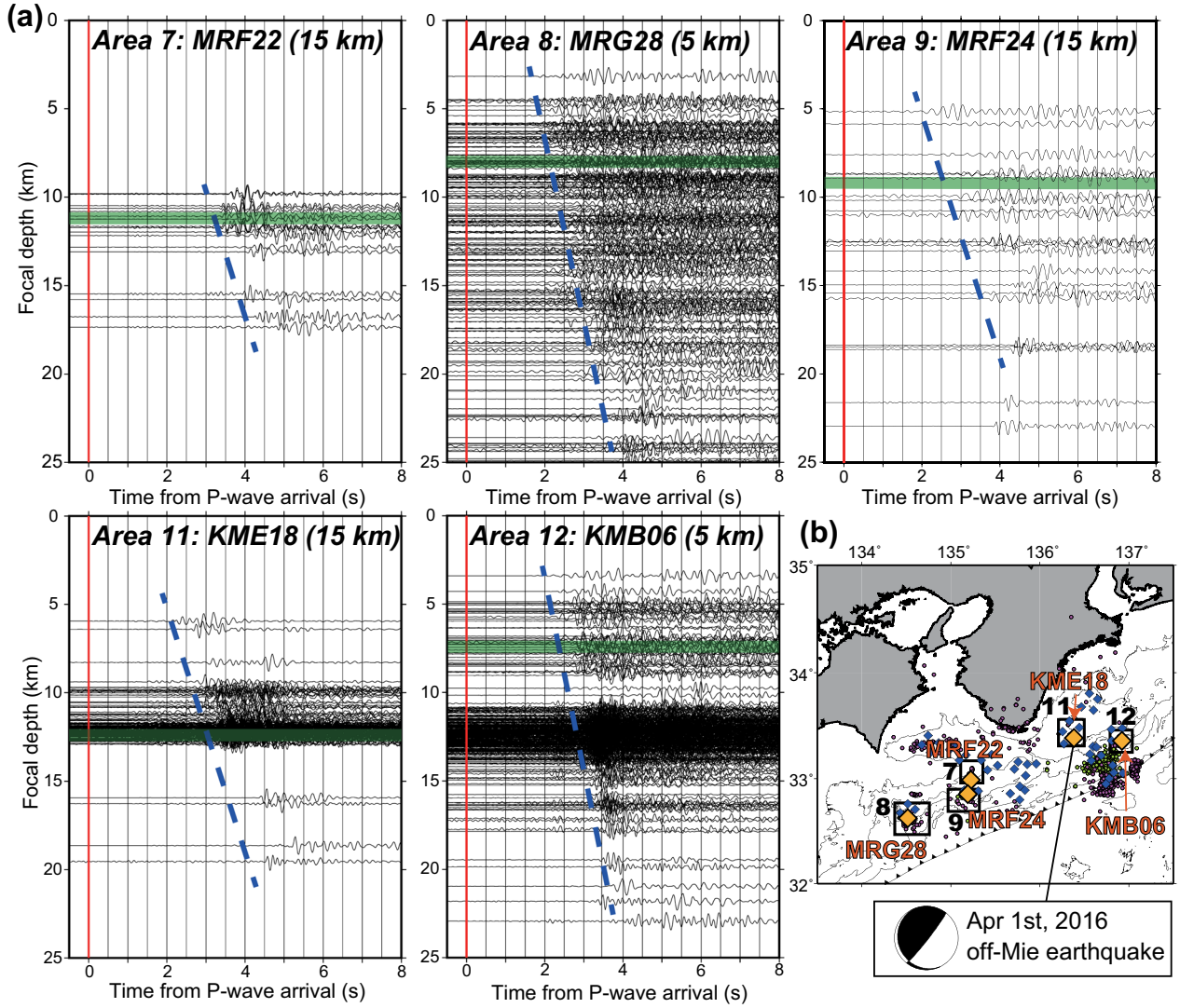


**Fig. 14** Observed waveforms in the vicinity of each station. **a** Examples of the observed waveform (horizontal component) whose focal depth is larger than the epicentral distance with respect to the hypocenter depth. The maximum epicentral distance for each station is shown in each figure. All waveforms are aligned by the P-wave arrival time. Blue lines show the approximate straight line of the S-wave arrival time. The thick green line shows the depth of the plate interface beneath each station. **b** Station locations shown in **a**. The focal mechanism solution for the 2016 off-Mie earthquake is also shown

the JMA catalog without distinction between interplate and intraplate earthquakes (Nanjo and Yoshida 2018).

## 5 Conclusions

Simultaneous estimation of 3-D seismic wave velocity structure and hypocenter relocation in the Nankai Trough of the Kii Peninsula was performed using both onshore and offshore observation network data to investigate the spatiotemporal distribution of interplate earthquakes and their relationship with interplate coupling and slow earthquakes. First, the estimated velocity model revealed three large structural heterogeneities, indicated by previous studies: high-velocity plutonic rocks beneath Cape Shionomisaki, a subducted seamount off Muroto, and the subducted Paleo-Zenith Ridge. Moreover, our velocity model indicated the absence of other subducted seamounts, whose spatial scale was similar or larger than the subducted seamount off Muroto. Second, the hypocenter relocation unraveled the existence of patch-like interplate seismicity zones. Most of such zones were located within the seismogenic zone depth, outside both the strong interplate coupling areas and high (> 1.9) Vp/

Vs areas along the plate interface. In addition, several zones of interplate seismicity overlapped with the area where slow earthquakes were observed. Third, the spatiotemporal comparisons of interplate seismicity and slow earthquakes in these areas suggested that interplate seismicity occurred in conjunction with SSE. Overall, regular microearthquake observations in the megathrust seismogenic zone should strengthen the detailed monitoring of the stick–slip behavior along the plate interface.

#### Abbreviations

SSE: Slow-slip event; VLFE: Very-low-frequency earthquake; DONET: Dense Oceanfloor Network system for Earthquakes and Tsunamis; 3-D: Three-dimensional; STA: Short-time average; LTA: Long-time average; CRT: Checkerboard resolution test; DWS: Derivative weighted sum; JMA: Japan Meteorological Agency; SIC: Shionomisaki igneous complex.

#### Acknowledgements

We would like to thank the editor Yuji Yagi and two anonymous reviewers for suggestions and comments. We also thank the JMA for providing the unified earthquake catalogue, waveforms, and arrival-time data for the seismic stations of JMA, National Research Institute for Earth Science and Disaster Resilience (NIED), Univ. of Tokyo, Kyoto Univ., Nagoya Univ., Kochi Univ., and National Institute of Advanced Industrial Science and Technology. We appreciate the effort of Drs. Shinichiro Kamiya, Masaru Nakano, Takeshi Nakamura, Mamoru Hyodo, and Mr. Kensuke Suzuki for event detection and manual phase picking. All figures were prepared using Generic Mapping Tools (Wessel and Smith 1991). A portion of the slow earthquake catalog used in this study was downloaded from the "Slow Earthquake Database (http://www-solid.eps.s.u-tokyo.ac.jp/~sloweq/; Kano et al. 2018)," which was supported by JSPS KAKENHI Grant Number JP16H06472 in Scientific Research on Innovative Areas "Science of Slow Earthquakes."

#### Author contributions

YY contributed to formal analysis, investigation, methodology, and writing of the original draft. SY was involved in data curation, investigation, and resources. KA and TH contributed to review and editing. NT was involved in conceptualization, review, and editing. All authors read and approved the final manuscript.

#### Funding

Not applicable.

#### Availability of data and materials

The JMA Unified catalog and first-arrival time data are available at https://www.hinet.bosai.go.jp. Online waveform data used in this study are available at https://doi.org/10.17598/NIED.0003. https://doi.org/10.17598/NIED.0005, and https://doi.org/10.17598/NIED.0008 (National Research Institute for Earth Science and Disaster Resilience 2019a, b, c). The offline data used in this study are available at https://doi.org/10.17596/0002069 (JAMSTEC 2004).

## Declarations

#### Competing interests

The authors declare that they have no competing interest.

#### Author details

[1]Japan Agency for Marine-Earth Science and Technology, 3173-25 Showa-machi, Kanazawa-ku, Yokohama, Kanagawa 236-0001, Japan. [2]National Research Institute for Earth Science and Disaster Resilience, 3-1 Tennodai, Tsukuba, Ibaraki 305-0006, Japan.

Received: 6 April 2022 Accepted: 25 May 2022
Published: 3 June 2022

#### References

Akuhara T, Mochizuki K, Kawakatsu H, Takeuchi N (2017) A fluid-rich layer along the Nankai trough megathrust fault off the Kii Peninsula inferred from receiver function inversion. J Geophys Res Solid Earth 122(8):6524–6537. https://doi.org/10.1002/2017jb013965

Ando M (1975) Source mechanisms and tectonic significance of historical earthquakes along the Nankai trough, Japan. Tectonophysics 27:119–140

Araki E, Saffer DM, Kopf AJ, Wallace LM, Kimura T, Machida Y, Ide S, Davis E, IODP Expedition 365 shipboard scientists (2017) Recurring and triggered slow-slip events near the trench at the Nankai Trough subduction megathrust. Science 356(6343):1157–1160. https://doi.org/10.1126/science.aan3120

Argus DF, Gordon RG, DeMets C (2011) Geologically current motion of 56 plates relative to the no-net-rotation reference frame. Geochem Geophys Geosyst. https://doi.org/10.1029/2011gc003751

Ariyoshi K, Iinuma T, Nakano M, Kimura T, Araki E, Machida Y, Sueki K, Yada S, Nishiyama T, Suzuki K, Hori T, Takahashi N, Kodaira S (2021) Characteristics of slow slip event in march 2020 revealed from borehole and DONET observatories. Front Earth Sci 8:66. https://doi.org/10.3389/feart.2020.600793

Arnulf AF, Bassett D, Harding AJ, Kodaira S, Nakanishi A, Moore G (2022) Upper-plate controls on subduction zone geometry, hydration and earthquake behaviour. Nat Geosci 15:143–148. https://doi.org/10.1038/s41561-021-00879-x

Baba T, Cummins PR (2005) Contiguous rupture areas of two Nankai Trough earthquakes revealed by high-resolution tsunami waveform inversion. Geophys Res Lett 32:L08305. https://doi.org/10.1029/2004GL022320

Bartlow NM, Wallace LM, Beavan RJ, Bannister S, Segall P (2014) Time-dependent modeling of slow slip events and associated seismicity and tremor at the Hikurangi subduction zone, New Zealand. J Geophys Res Solid Earth 119(1):734–753. https://doi.org/10.1002/2013jb010609

Bird P (2003) An updated digital model of plate boundaries. Geochem Geophys Geosyst 4(3):66. https://doi.org/10.1029/2001gc000252

Fukuda J (2018) Variability of the space-time evolution of slow slip events off the Boso Peninsula, Central Japan, From 1996 to 2014. J Geophys Res Solid Earth 123(1):732–760. https://doi.org/10.1002/2017jb014709

Gutenberg B, Richter CF (1956) Earthquake magnitude, intensity, energy and acceleration. Bull Seismol Soc Am 46:105–146

Hashimoto C, Fukui K, Matsu'ura M (2004) 3-D modeling of plate interfaces and numerical simulation of long-term crustal deformation in and around Japan. Pure Appl Geophys 161:2053–2068. https://doi.org/10.1007/s00024-004-2548-8

Hayes GP, Moore GL, Portner DE, Hearne M, Flamme H, Furtney M, Smoczyk GM (2018) Slab2, a comprehensive subduction zone geometry model. Science 362:58–61. https://doi.org/10.1126/science.aat4723

Hirose F, Nakajima J, Hasegawa A (2008) Three-dimensional seismic velocity structure and configuration of the Philippine Sea slab in southwestern Japan estimated by double-difference tomography. J Geophys Res 113:B09315. https://doi.org/10.1029/2007JB005274

Hirose H, Matsuzawa T, Kimura T, Kimura H (2014) The Boso slow slip events in 2007 and 2011 as a driving process for the accompanying earthquake swarm. Geophys Res Lett 41(8):2778–2785. https://doi.org/10.1002/2014gl059791

Honda R, Kono Y (2005) Buried large block revealed by gravity anomalies in the Tonankai and Nankai earthquakes regions, southwestern Japan. Earth Planets Space 57:e1–e4

Horiuchi S, Horiuchi Y, Yamamoto S, Nakamura H, Wu C, Rydelek PA, Kachi M (2009) Home seismometer for earthquake early warning. Geophys Res Lett 36(3):66. https://doi.org/10.1029/2008gl036572

Hyndman RD, Peacock SM (2003) Serpentinization of the forearc mantle. Earth Planet Sci Lett 212(3–4):417–432. https://doi.org/10.1016/s0012-821x(03)00263-2

Hyndman RD, Yamano M, Oleskevich DA (1997) The seismogenic zone of subduction thrust faults. Island Arc 6(3):244–260. https://doi.org/10.1111/j.1440-1738.1997.tb00175.x

Igarashi T (2020) Catalog of small repeating earthquakes for the Japanese Islands. Earth Planets Space 72(1):66. https://doi.org/10.1186/s40623-020-01205-2

Ito Y, Obara K, Shiomi K, Sekine S, Hirose H (2007) Slow earthquakes coincident with episodic tremors and slow slip events. Science 315:503–506. https://doi.org/10.1126/science.1134454

Ito A, Tonegawa T, Uchida N, Yamamoto Y, Suetsugu D, Hino R, Sugioka H, Obana K, Nakahigashi K, Shinohara M (2019) Configuration and structure of the Philippine Sea Plate off Boso, Japan: constraints on the shallow subduction kinematics, seismicity, and slow slip events. Earth Planets Space 71(1):66. https://doi.org/10.1186/s40623-019-1090-y

JAMSTEC (2004) JAMSTEC Seismic Survey Database, JAMSTEC. https://doi.org/10.17596/0002069. Accessed 23 May 2022

Japan Meteorological Agency (2022) List of earthquakes **(in Japanese)**. https://www.data.jma.go.jp/svd/eqev/data/daily_map/index.html. Accessed 2 Apr 2022

Kanamori H (1972) Tectonic implications of the 1944 Tonankai and the 1946 Nankaido earthquakes. Phys Earth Planet Inter 5:129–139

Kaneda Y, Kawaguchi K, Araki E, Matsumoto H, Nakamura T, Kamiya S, Ariyoshi K, Hori T, Baba T, Takahashi N (2015) Development and application of an advanced ocean floor network system for megathrust earthquakes and tsunamis. In: Seafloor observatories. Springer, Heidelberg, pp 6433–666. https://doi.org/10.1007/978-3-642-11374-1_252

Kano M, Aso N, Matsuzawa T, Ide S, Annoura S, Arai R, Baba S, Bostock M, Chao K, Heki K, Itaba S, Ito Y, Kamaya N, Maeda T, Maury J, Nakamura M, Nishimura T, Obana K, Ohta K, Poiata N, Rousset B, Sugioka H, Takagi R, Takahashi T, Takeo A, Tu Y, Uchida N, Yamashita Y, Obara K (2018) Development of a slow earthquake database. Seismol Res Lett 89(4):1566–1575. https://doi.org/10.1785/0220180021

Kawaguchi K, Kaneko S, Nishida T, Komine T (2015) Construction of the DONET real-time seafloor observatory for earthquakes and tsunami monitoring, In Seafloor observatories. Springer, Heidelberg, pp 211–228. https://doi.org/10.1007/978-3-642-11374-1_10.

Kimura G, Hashimoto Y, Kitamura Y, Yamaguchi A, Koge H (2014) Middle Miocene swift migration of the TTT triple junction and rapid crustal growth in southwest Japan: a review. Tectonics 33:1219–1238. https://doi.org/10.1002/2014TC003531

Kobayashi A (2014) A long-term slow slip event from 1996 to 1997 in the Kii Channel. Jpn Earth Planets Space. https://doi.org/10.1186/1880-5981-66-9

Kodaira S, Takahashi N, Nakanishi A, Miura S, Kaneda Y (2000) Subduction seamount imaged in the rupture zone of the 1946 Nankaido earthquake. Science 289:104–106. https://doi.org/10.1126/science.289.5476.104

Kodaira S, Kurashimo E, Park J-O, Takahashi N, Nakanishi A, Miura S, Iwasaki T, Hirata N, Ito K, Kaneda Y (2002) Structural factors controlling the rupture process of a megathrust earthquake at the Nankai trough seismogenic zone. Geophys J Int 149:815–835

Kodaira S, Hori T, Ito A, Miura S, Fujie G, Park J-O, Baba T, Sakaguchi H, Kaneda Y (2006) A cause of rupture segmentation and synchronization in the Nankai trough revealed by seismic imaging and numerical simulation. J Geophys Res 111:B09301. https://doi.org/10.1029/2005JB004030

Maeda T, Obara K (2009) Spatio-temporal distribution of seismic energy radiation from low-frequency tremor in western Shikoku, Japan. J Geophys Res, 114:B00A09. https://doi.org/10.1029/2008JB006043.

Matsubara M, Sato H, Ishiyama T, Van Horne AD (2017) Configuration of the Moho discontinuity beneath the Japanese Islands derived from three-dimensional seismic tomography. Tectonophysics 710–711:97–107. https://doi.org/10.1016/j.tecto.2016.11.025

Matsuzawa T, Hirose H, Shibazaki B, Obara K (2010) Modeling short- and long-term slow slip events in the seismic cycles of large subduction earthquakes. J Geophys Res 115:B12301. https://doi.org/10.1029/2010JB007566

Mochizuki K, Nakahigashi K, Kuwano A, Yamada T, Shinohara M, Sakai S, Kanazawa T, Uehira K, Shimizu H (2010) Seismic characteristics around the fault segment boundary of historical great earthquakes along the Nankai Trough revealed by repeated long-term OBS observations. Geophys Res Lett 37:L09304. https://doi.org/10.1029/2010GL042935

Moreno M, Haberland C, Oncken O, Rietbrock A, Angiboust S, Heidbach O (2014) Locking of the Chile subduction zone controlled by fluid pressure before the 2010 earthquake. Nat Geosci 7(4):292–296. https://doi.org/10.1038/ngeo2102

Murotani S, Shimazaki K, Koketsu K (2015) Rupture process of the 1946 Nankai earthquake estimated using seismic waveforms and geodetic data. J Geophys Res Solid Earth 120:5677–5692. https://doi.org/10.1002/2014JB011676

Nakamura Y, Shiraishi K, Fujie G, Kodaira S, Kimura G, Kaiho Y, No T, Miura S (2022) Structural anomaly at the boundary between strong and weak plate coupling in the Central-Western Nankai Trough. Geophys Res Lett. https://doi.org/10.1029/e2022GL098180

Nakanishi A, Takahashi N, Yamamoto Y, Takahashi T, Ozgur CS, Nakamura T, Obana K, Kodaira S, Kaneda Y (2018) Three-dimensional plate geometry and P-wave velocity models of the subduction zone in SW Japan: implications for seismogenesis. In: Geology and tectonics of subduction zones: a tribute to Gaku Kimura. https://doi.org/10.1130/2018.2534(04)

Nakano M, Nakamura T, Kaneda Y (2015) Hypocenters in the Nankai Trough determined by using data from both ocean-bottom and land seismic networks and a 3D velocity structure model: implications for seismotectonic activity. Bull Seismo Soc Am 105:1594–1605. https://doi.org/10.1785/0120140309

Nakano M, Hori T, Araki E, Kodaira S, Ide S (2018a) Shallow very-low-frequency earthquakes accompany slow slip events in the Nankai subduction zone. Nat Commun 9(1):984. https://doi.org/10.1038/s41467-018-03431-5

Nakano M, Hyodo M, Nakanishi A, Yamashita M, Hori T, Kamiya S, Suzuki K, Tonegawa T, Kodaira S, Takahashi N, Kaneda Y. (2018b) The 2016 Mw 5.9 earthquake off the southeastern coast of Mie Prefecture as an indicator of preparatory processes of the next Nankai Trough megathrust earthquake. Prog Earth Planet Sci. https://doi.org/10.1186/s40645-018-0188-3

Nanjo KZ, Yoshida A (2018) A b map implying the first eastern rupture of the Nankai Trough earthquakes. Nat Commun 9(1):1117. https://doi.org/10.1038/s41467-018-03514-3

National Research Institute for Earth Science and Disaster Resilience (2019a) NIED Hi-net, National Research Institute for Earth Science and Disaster Resilience. https://doi.org/10.17598/NIED.0003

National Research Institute for Earth Science and Disaster Resilience (2019b) NIED F-net, National Research Institute for Earth Science and Disaster Resilience. https://doi.org/10.17598/NIED.0005

National Research Institute for Earth Science and Disaster Resilience (2019c) NIED DONET, National Research Institute for Earth Science and Disaster Resilience. https://doi.org/10.17598/NIED.0008

Nishimura T, Yokota Y, Tadokoro K, Ochi T (2018) Strain partitioning and interplate coupling along the northern margin of the Philippine Sea plate, estimated from Global Navigation Satellite System and Global Positioning System-Acoustic data. Geosphere 14(2):535–551. https://doi.org/10.1130/ges01529.1

Noda A, Saito T, Fukuyama E (2018) Slip-deficit rate distribution along the Nankai Trough, Southwest Japan, with elastic lithosphere and viscoelastic asthenosphere. J Geophys Res Solid Earth 123(9):8125–8142. https://doi.org/10.1029/2018jb015515

Obara K (2002) Nonvolcanic deep tremor associated with subduction in southwest Japan. Science 296(5573):1679–1681. https://doi.org/10.1126/science.1070378

Obara K, Kato A (2016) Connecting slow earthquakes to huge earthquakes. Science 353(6296):253–257. https://doi.org/10.1126/science.aaf1512

Obara K, Tanaka S, Maeda T, Matsuzawa T (2010) Depth-dependent activity of non-volcanic tremor in southwest Japan. Geophy Res Lett 37:L13306. https://doi.org/10.1029/2010GL043679

Oleskevich DA, Hyndman RD, Wang K (1999) The updip and downdip limits to great subduction earthquakes: Thermal and structural models of Cascadia, south Alaska, SW Japan, and Chile. J Geophys Res Solid Earth 104(B7):14965–14991. https://doi.org/10.1029/1999JB900060

Park J-O, Moore GF, Tsuru T, Kodaira S, Kaneda Y (2004) A subducted oceanic ridge influencing the Nankai megathrust earthquake rupture. Earth Planet Sci Lett 217(1–2):77–84. https://doi.org/10.1016/s0012-821x(03)00553-3

Qin Y, Fujie G, Kodaira S, Nakamura Y, Kaiho Y, No T, Obana K, Miura S (2021) High-density seismic refraction imaging of plate-boundary structures in the slow earthquake gap zone off Western Kii Peninsula, Nankai Trough. Geophys Res Lett. https://doi.org/10.1029/2020gl089132

Sakai S, Yamada T, Shinohara M, Hagiwara H, Kanazawa T, Obana K, Kodaira S, Kaneda Y (2005) Urgent aftershock observation of the 2004 off the Kii Peninsula earthquake using ocean bottom seismometers. Earth Planets Space 57(4):363–368. https://doi.org/10.1186/Bf03352577

Shaddox HR, Schwartz SY (2019) Subducted seamount diverts shallow slow slip to the forearc of the northern Hikurangi subduction zone. N Z Geol 47(5):415–418. https://doi.org/10.1130/G45810.1
Sholtz CH (2002) The mechanics of earthquakes and faulting. Cambridge University Press, Cambridge. https://doi.org/10.1017/CBO9780511818516
Snoke JA (2003) FOCMEC: FOCal MEChanism determinations. In: Lee WHK et al (eds) International handbook of earthquake and engineering seismology. Academic Press, Amsterdam, pp 1629–1630
Sugioka H, Okamoto T, Nakamura T, Ishihara Y, Ito A, Obana K, Kinoshita M, Nakahigashi K, Shinohara M, Fukao Y (2012) Tsunamigenic potential of the shallow subduction plate boundary inferred from slow seismic slip. Nat Geosci 5(6):414–418. https://doi.org/10.1038/NGEO1466
Takemura S, Noda A, Tonegawa T, Kubota T, Asano Y, Matsuzawa T, Shiomi K (2019) Migrations and clusters of shallow very low frequency earthquakes in the regions surrounding shear stress accumulation peaks along the Nankai Trough. Geophys Res Lett 46:11830–11840. https://doi.org/10.1029/2019GL084666
The Headquarters for Earthquake Research Promotion (2022) List of long-term evaluations **(in Japanese)**, https://www.jishin.go.jp/main/choukihyoka/ichiran.pdf. Accessed 2 April 2022
Thorwart M, Dzierma Y, Rabbel W, Hensen C (2013) Seismic swarms, fluid flow and hydraulic conductivity in the forearc offshore North Costa Rica and Nicaragua. Int J Earth Sci 103(7):1789–1799. https://doi.org/10.1007/s00531-013-0960-y
Thurber CH, Eberhart-Phillips D (1999) Local earthquake tomography with flexible gridding. Comput Geosci 25:809–818
Toh A, Chen WJ, Takeuchi N, Dreger DS, Chi WC, Ide S (2020) Influence of a subducted oceanic ridge on the distribution of shallow VLFEs in the Nankai Trough as revealed by moment tensor inversion and cluster analysis. Geophys Res Lett. https://doi.org/10.1029/2020gl087244
Urabe T, Tsukada S (1992) Win—a workstation program for processing waveform data from microearthquake networks. Prog Abst Seismol Soc Jpn 2:41 **(in Japanese)**
Vaca S, Vallée M, Nocquet J-M, Battaglia J, Régnier M (2018) Recurrent slow slip events as a barrier to the northward rupture propagation of the 2016 Pedernales earthquake (Central Ecuador). Tectonophysics 724–725:80–92. https://doi.org/10.1016/j.tecto.2017.12.012
Watanabe H (1971) Determination of earthquake magnitude at regional distance in and near Japan. Zisin2 24:189–200 **(in Japanese with English abstract)**
Wessel P, Smith WHF (1991) Free software helps map and display data. Eos Trans AGU 72:441
Yamamoto Y, Takahashi T, Kaiho Y, Obana K, Nakanishi A, Kodaira S, Kaneda Y (2017) Seismic structure off the Kii Peninsula, Japan, deduced from passive- and active-source seismographic data. Earth Planet Sci Lett 461:163–175. https://doi.org/10.1016/j.epsl.2017.01.003
Yamamoto Y, Takahashi T, Ishihara Y, Kaiho Y, Arai R, Obana K, Nakanishi A, Miura S, Kodaira S, Kaneda Y (2018) Modeling the geometry of plate boundary and seismic structure in the Southern Ryukyu Trench Subduction Zone, Japan, using amphibious seismic observations. J Geophys Res Solid Earth 123(2):1793–1809. https://doi.org/10.1002/2017jb015330
Yamamoto Y, Takahashi T, Ishihara Y, Obana K, Miura S, Kodaira S, Kaneda Y (2020) Plate geometry model and seismicity in the northern Ryukyu subduction zone, Japan, deduced from amphibious seismic observations. Earth Planet Sci Lett. https://doi.org/10.1016/j.epsl.2020.116143
Yamamoto Y, Ariyoshi K, Yada S, Nakano M, Hori T (2022) Spatio-temporal distribution of shallow very-low-frequency earthquakes between December 2020 and January 2021 in Kumano-nada, Nankai subduction zone, detected by a permanent seafloor seismic network. Earth Planets Space. https://doi.org/10.1186/s40623-022-01573-x
Yokota Y, Ishikawa T (2020) Shallow slow slip events along the Nankai Trough detected by GNSS-A. Sci Adv 6(3):eaay5786. https://doi.org/10.1126/sciadv.aay5786
Yokota Y, Ishikawa T, Watanabe S, Tashiro T, Asada A (2016) Seafloor geodetic constraints on interplate coupling of the Nankai Trough megathrust zone. Nature. https://doi.org/10.1038/nature17632
Zhang H, Thurber C (2006) Development and applications of double-difference seismic tomography. Pure Appl Geophys 163:373–403
Zhao D, Huang Z, Umino N, Hasegawa A, Kanamori H (2011) Structural heterogeneity in the megathrust zone and mechanism of the 2011 Tohoku-oki earthquake (Mw 9.0). Geophys Res Lett 38:L17308. https://doi.org/10.1029/2011GL048408

## Publisher's Note